Title: **Influenza Virus Uses Transportin 1 for vRNP Debundling During Cell Entry**

Authors: Yasuyuki Miyake[1,4], Jeremy Keusch[3], Laure Decamps[2†], Hung Ho-Xuan[2†], Sho Iketani[1], Heinz Gut[3], Ulrike Kutay[2], Ari Helenius[2], Yohei Yamauchi[1*]

Affiliations:

[1] School of Cellular and Molecular Medicine, Faculty of Life Sciences, University of Bristol, University Walk, Bristol, BS8 1TD, UK.

[2] Institute of Biochemistry, ETH Zurich, Otto-Stern-Weg 3, CH-8093, Zurich, Switzerland.

[3] Friedrich Miescher Institute for Biomedical Research, Maulbeerstrasse 66, 4058 Basel, Switzerland

[4] Department of Virology, Nagoya University Graduate School of Medicine, 65 Tsurumai-cho, Showa-ku, Nagoya 466-8550, Aichi, Japan.

*Correspondence to: yohei.yamauchi@bristol.ac.uk

†These authors contributed equally to this work.

Influenza A virus (IAV) is a pathogen of great medical impact. To develop novel antiviral strategies, it is essential to understand molecular aspects of virus-host cell interactions in detail. During entry, the viral ribonucleoproteins (vRNPs) that carry the RNA genome must be released from the incoming particle before they can enter the nucleus for replication. The uncoating process is facilitated by histone deacetylase 6 (HDAC6)[1]. However, the precise mechanism of shell opening and vRNP debundling is unknown. Here we show that transportin1 (TNPO1), a member of importin β family proteins, binds to a PY-NLS [2] sequence motif close to the N-terminus of matrix protein (M1) exposed during acid-priming of the viral core. It promotes the removal of M1 and induces disassembly of vRNP bundles. Next, the vRNPs interact with importin α/β (KPNA/KPNB1) and enter the nucleus. Thus, IAV uses dual importin βs for distinct steps in host cell entry.

In the IAV particle, the eight single-stranded, negative-sense RNAs that make up the genome are individually packaged with a viral polymerase complex into helical vRNPs in which the major protein is the nucleoprotein, NP. Together with the matrix protein, M1, the vRNPs form a stable, supra-macromolecular complex, the viral core, in which M1 provides a rigid shell around a bundle of vRNPs [3]. The uncoating process is initiated in early and maturing endosomes or macropinosomes after endocytosis of incoming virus particles [4, 5]. The M2 ion channel in the viral envelope allows exposure of the capsid to low pH and elevated K^+, which results in loosening of interactions within the M1 core and between vRNPs in a process called priming [6]. Penetration of the primed core into the cytosol occurs by low pH-triggered, hemagglutinin(HA)-mediated membrane fusion in late endosomes (LEs) [7-9]. In the cytosol, the M1 shell dissociates, and vRNPs are imported into the nucleus [10-15]. In the nucleus, the vRNPs are distributed as discrete complexes separated from each other [16]. Thus, IAV uncoating involves three major steps; priming, M1 shell disassembly, and vRNP debundling.

We have previously shown that histone deacetylase 6 (HDAC6) serves as a key cellular factor in the M1

shell disassembly step [1]. It binds to unanchored ubiquitin chains and M1 exposed as viral cores emerge on the cytosolic surface of LEs. It connects the M1 shell to cytoskeleton motors dynein and myosin II, which promote disassembly of the shell by a cytoskeleton-dependent mechanism related to aggresome processing. The vRNPs are released into the cytosol where KPNA/KPNB1 mediate their nuclear uptake via nuclear pore complexes [1, 10, 17].

To identify additional host proteins involved in the cytosolic uncoating and nuclear import steps, we performed an infection screen using an siRNA library against 70 nuclear pore proteins and genes known to regulate nucleocytoplasmic transport (**Fig.1a and Supplementary Fig. 1**) [18-20]. We found that infection was reduced in cells depleted of the nuclear import/export factors CAS (cellular apoptosis susceptibility protein)/XPO2, KPNB1 (karyopherin-β1, importin β), and several nuclear pore proteins that have been previously identified as essential for infection (**Supplementary Fig. 1**)[21]. Among the novel hits, nuclear import factor transportin 1 (TNPO1, also known as karyopherin-β2 or Kapβ2) caught our interest because it is a well-characterised receptor for nuclear import of cellular ribonucleoprotein complexes and RNA-binding proteins such as hnRNP A1 [22, 23] many of which carry a recognition sequence termed PY-NLS [2, 24].

Depletion of TNPO1 using siRNA (TNPO1#2) or shRNA reduced the number of infected cells by 66-79% in A549 and MDCK cells (**Fig. 1b-d**). Production of infectious virus was reduced by 81% in MDCK cells (**Fig. 1e**). Infection could be rescued by expression of TNPO1 using an siRNA-insensitive construct (GFP-TNPO1, **Fig. 1f**). TNPO1 was needed across various IAV strains X31 (H3N2), WSN (H1N1), and Udorn (H3N2) of spherical and filamentous morphology (**Fig. 1g**). TNPO1 was, moreover, required for X31 infection in HeLa cells (**Supplementary Fig. 2**).

To define the virus entry step(s) that require TNPO1, we first analysed the intracellular location of incoming M1 and vRNPs by indirect immunofluorescence (IIF) in control A549 cells at different times after virus internalisation. At 3hpi, uncoating of the M1 shell had already occurred judging by the broad distribution of M1 throughout the cytoplasm (**Fig. 2a**). At 4hpi, NP staining occurred almost exclusively in the nucleus **(Fig. 2b)**. This indicated that at 3-4hpi the majority of cores had lost their M1 shell and vRNPs had been released, debundled, and nuclear imported.

That debundling of vRNPs could, at least in part, occur in the cytoplasm prior to nuclear import was shown by structured illumination microscopy (SIM) (**Fig. 2c**). Images taken 1h after synchronised release of vRNPs from LEs in MEFs showed that in addition to large bright spots containing NP, smaller uniform NP-containing spots of low brightness were present in the cytoplasm. That these were similar in brightness and size to the spots in the nucleus known to represent individual vRNPs [16, 25], suggested that debundling of vRNPs can and does take place in the cytoplasm.

In TNPO1-depleted cells, M1 was present in bright, cytoplasmic spots. The majority of NP also remained in cytoplasmic spots that had a distribution similar to viruses trapped by bafilomycin A1 (Baf A1)-treatment in endosomes (**Fig. 2c**). Thus, M1 uncoating, vRNP debundling, and vRNP nuclear import were all inhibited in cells depleted of TNPO1.

Triple-staining of TNPO1-depleted and KPNB1-depleted cells 2.5hpi provided evidence for a previously undetected step in the uncoating process; the release of uncoated or partially coated cores from LEs into the cytosol (**Fig. 2d-g**). In TNPO1-depleted cells at this time point, NP staining was mainly cytoplasmic and present in spots of medium brightness that contained variable amounts of M1. Many of these spots did not colocalise with LAMP1; a marker for endolysosomes (**Fig. 2d**). In KPNB1-depleted cells, NP-positive spots of different brightness were also distributed throughout the cytosol, and they did not colocalise with LAMP1. When cores were synchronously released from LEs in TNPO1-depleted cells [1] and analysed after

30 min, many of the cytoplasmic NP spots contained M1 in contrast to control cells that displayed small NP spots in the nucleus or larger spots in the cytoplasm devoid of M1 (**Supplementary Fig. 3**). Taken together, these results indicated that TNPO1 is required for a step involving removal of M1 from cores that have been released into the cytosol.

Judging by the brightness of the NP-positive spots in TNPO1-depleted cells compared to nuclear vRNPs in control cells, the vRNPs were still associated with each other. When KPNB1 was depleted, vRNPs failed to enter the nucleus [15, 16, 21] but uncoating of cytoplasmic cores proceeded further than in TNPO1-depleted cells; M1 was no longer associated with NP-containing spots (**Fig. 2d**). The smaller spot size indicated that vRNPs had been debundled (**Fig. 2d, f**). Taken together, these results indicated that TNPO1 removed M1 from incoming cores and debundled the vRNPs in the cytosol. While KPNB1 is clearly essential for nuclear import [16, 21], it was dispensable for core uncoating and debundling.

Next, we used synchronised penetration of cores into the cytosol of A549 cells by inducing fusion of pre-primed, cell surface-bound viruses with the plasma membrane (acid-bypass) [6, 26] (**Supplementary Fig. 4a**). Fusion/hemifusion was confirmed by lipid mixing [25]. Depletion of TNPO1 and KPNB1 inhibited vRNP import by 68% and 79%, respectively **(Fig. 2h**, **Supplementary Fig. 4b**). In half of TNPO1-depleted cells M1-uncoating failed to occur (**Fig. 2h, Supplementary Fig. 4a**). In TNPO1-depleted MDCK cells, M1-uncoating was reduced by 75% compared to control cells but fusion/hemifusion was unaffected (**Fig. 2i, j**). M1-uncoating could be rescued by ectopic expression of shRNA-insensitive GFP-human TNPO1 (**Fig. 2k**). Taken together, these findings confirmed that TNPO1 was involved in the dissociation of M1 from incoming cores, whereas KPNB1 nuclear imported vRNPs [21]. In further support of a role for TNPO1 in M1-uncoating, overexpression of TNPO1 increased M1-uncoating (**Supplementary Fig. 4c**), and that of a recombinant protein carrying the hnRNP A1 M9-NLS [22, 23] caused a reduction (**Supplementary Fig. 4c**). We concluded that TNPO1's role in the dissociation of M1 from incoming cores was associated with the PY-NLS binding function.

IIF showed that TNPO1 in control cells is localised in the nucleus with a few spots in the cytoplasm (**Fig. 3a**). Fifteen min after synchronous release of particles from LEs in MEFs [1], we could observe that some of the NP-containing spots in the cytoplasm contained TNPO1 (**Fig. 3a, WT**). Spots were also weakly stained for M1. This indicated that TNPO1 associates with incoming cores and with vRNP bundles that have residual M1. That TNPO1 also colocalised with M1/NP-positive spots in HDAC6 -/- MEFs (**Fig. 3a, HDAC6 -/-**) indicated that TNPO1 association with cores takes place in the absence of HDAC6 and aggresome processing. In these spots, the staining for M1 was stronger suggesting that TNPO1 can bind to more intact-looking cores but is unable to remove M1 efficiently without HDAC6 action.

When virus was primed at pH 5.6 and 120 mM KCl, lysed, incubated with His-TNPO1 for pull-down, M1 was found to co-precipitate (**Fig. 3b**). However, only trace amounts were precipitated from lysates prepared from unprimed virus. When cells were infected for 2.5h in the presence or absence of NH_4Cl, M1 co-precipitated less efficiently with TNPO1 in the NH_4Cl-treated cells compared to non-treated cells (**Supplementary Fig. 5a, b**).

When examining the amino acid sequence of M1, we observed short sequences close to the N-terminus that resemble known elements to the PY-NLSs recognised by TNPO1 in cellular substrates [27]. These elements are referred to as epitopes 1, 2, and 3 (**Fig. 3c),** of which the glycine residue in epitope 1 is critical for TNPO1 recognition [2]. Sequences similar to epitopes 1 and 2 are conserved among M1 of IAV strains. The crystal structure of M1[28] shows that they are on the surface of M1. We hypothesised that in primed cores, they may serve as a binding motif for TNPO1. The hypothesis was tested by generating a mutant IAV WSN (H1N1) strain in which Gly 18 in M1 was replaced with alanine by reverse genetics [29]. When normalised for the same number of viruses, the G18A mutant virus reached 2% of the infectivity observed for the WT virus (**Fig. 3d**).

When His-TNPO1 was pulled-down after incubation with pre-primed virus lysates containing either the G18A virus or the WT control virus, the M1 of G18A precipitated less efficiently (**Fig. 3e**). This indicated that Gly 18 is essential not only for infection but also for efficient TNPO1 association. We also found that Gly 18 is an epitope of the HB-64 monoclonal antibody used to detect M1-uncoating (**Supplementary Fig. 6**), indicating that acidification exposes the PY-NLS.

We solved the crystal structure of the neutral pH form of M1 with the G18A mutation expressed in *E. coli*, and compared it to the structure of the WT protein. The main difference between the WT structure was seen around the PY-NLS sequence motif. A cavity formed by loops L1 (15-19) and L3 (49-53) in WT M1 was absent in G18A (**Fig. 3f-h, Supplementary Fig. 7a, Supplementary Table 1**). The 1. 9 Å resolution G18A M1 N-terminal domain structure, though monomeric in solution, forms the so called face-to-back dimer in the crystal lattice representing the neutral pH oligomeric state of M1 similar to PDB entries 1EA3 or 5V8A [30, 31] (**Supplementary Fig. 7b)**. Glycine 18 and surrounding amino acid residues are masked in this face-to-back M1-M1 interface crystallised at neutral pH, but are exposed in acidified M1 crystals [28] **(Supplementary Fig.7c)**. This may explain why M1 in lysates of primed viruses engage TNPO1 better than unprimed ones (**Fig. 3b**). During virus entry, priming may thus allow subsequent TNPO1 binding to M1. It may explain why unprimed viruses are not uncoated [6] and why TNPO1 does not interfere with the functions of newly-synthesised M1 in infected cells.

In summary, our results lead to a more detailed step-by-step model for IAV uncoating **(Fig. 4)**. After viral uptake into endosomes, the M2 cation channels open resulting in influx of protons and K^+ ions that loosens interactions stabilising the core [6] and triggers a conformational change in M1 that exposes the PY-NLS close to the N-terminus. Following viral fusion in LEs, the core is exposed to cytosolic factors. HDAC6 binds to shell-associated, unanchored ubiquitin chains [1]. Together with other components of the aggresome processing machinery, HDAC6 releases the shell from the endosome surface and ruptures it. This process depends on forces generated by microtubules and microfilaments and the corresponding motors, dynein

and myosin II. At the same time, TNPO1 associates with the PY-NLS exposed in the primed M1. TNPO1's main role is to promote removal of vRNP-associated M1, which allows dissociation of vRNPs from each other. Some of the removed M1 may enter the nucleus with TNPO1. KPNA and KPNB1 bind to the classical NLS in NP resulting in nuclear import of fully or partially debundled vRNPs. Thus, the primary role of TNPO1 is M1 removal and debundling of vRNPs in the cytosol.

Acknowledgements

We thank Thomas Wild for help with siRNA screen preparation, Dominic Alibhai for image analysis, Tobias Schwarz for super-resolution microscopy, and Evgeny Onischenko for protein purification. This work was supported by the European Research Council (2-73905-09, Cellular biology of virus infection); Swiss National Science Foundation (2-77478-12, Regulation of early to late endosomal traffic)(A.H.), (31003A 166565, NCCR RNA&Disease)(U.K.), SystemsX VirX - A host-directed approach against viral disease (Y.Y. and H.G.). The Friedrich Miescher Institute for Biomedical Research is supported by the Novartis Research Foundation (J.K. and H.G.). Y.M. was funded by the Japan Society for the Promotion of Science (Research Fellowship for Young Scientists). Part of this work was performed at beamline X10SA of the Swiss Light Source.

Author Contributions

This study was conceptualised by Y.Y. and A.H., investigated by Y.M., J.K., L.D., H.H.-X., S.I., H.G., Y.Y., resources provided by U.K., the manuscript was written by Y.Y., Y.M., J.K., H.G., U.K., A.H., and reviewed by all.

Conflicting Interests

The authors have no conflicting interests to declare.

Materials and Methods

Cells

A549, Madin-Darby Canine Kidney (MDCK), HEK293T, and HeLa cells were obtained from the American Type Culture Collection (ATCC). Mouse embryonic fibroblasts (MEFs) were isolated from embryonic day 13.5 from male embryos of wild type and HDAC6 -/- mice [32]. For some acid-bypass experiments, the plate wells were coated with 0.01% poly-L-lysine prior to use. All cells were maintained in Dulbecco's modified Eagle's medium (DMEM)(Invitrogen), supplemented with 10% fetal calf serum (FCS) under 5% CO_2 at 37°C. MDCK cells capable of inducible expression of shRNA targeting the canine TNPO1 sequence GCAGTGCCTTTGCTACCTTAG was a kind gift from Ben L. Margolis [33].

Viruses

IAV X31 strain (an H3N2 reassorted strain derived from PR8 and A/Hong Kong/1/68 strains) was purchased from Virapur (CA, USA). To propagate X31 virus, 60 pathogen-free chicken eggs were inoculated with the virus and incubated at 33-37°C for 2 days. The allantoic fluid was harvested and clarified by low-speed centrifugation, which was then concentrated by high-speed centrifugation. To further concentrate the virus, two rounds of 10-40% sucrose gradient centrifugation were performed, viral bands harvested, pooled and re-suspended in formulation buffer (40% sucrose, 0.02% BSA, 20 mM HEPES pH 7.4, 100 mM NaCl, 2 mM $MgCl_2$). The viral titer was determined as 1.0 x10^{10} $TCID_{50}$ infectious units/ml in MDCK cells. The virus was aliquoted and stored in formulation buffer at -80℃ until use. IAV WSN

(A/WSN/1933) (H1N1) strain was propagated in MDCK cells and purified by sucrose gradient ultracentrifugation as previously described [6]. IAV Udorn (A/Udorn/72) (H3N2) strain was a kind gift from Jovan Pavlovic. $TCID_{50}$ assays were performed as described elsewhere.

Reagents

Hybridoma cell lines producing monoclonal antibodies specific for IAV M1 anti-M1 (HB-64) and NP (HB-65) were purchased from ATCC. Anti-IAV M1 (goat, #1311) was purchased from Virostat. Anti-TNPO1 (mouse, ab10303), anti-TNPO1 (rabbit, ab191539), anti-LAMP1 (rabbit, ab24170) antibodies were purchased from abcam, anti-CAS (sc-1708) from Santa Cruz. Anti-importin β (clone 31H4) monoclonal antibody was purchased from Sigma-Aldrich, anti-His monoclonal antibody from Sigma-Aldrich, anti-GFP monoclonal antibody (JL-8) from Clontech. The mouse monoclonal anti-A/WSN/33 HA (clone H15-B9-22 [34], The Wistar Institute, Philadelphia, US) was a kind gift from Silke Stertz. The anti-IAV M1/M2 monoclonal antibody (E10) was a kind gift from Jovan Pavlovic. Lipofectamine RNAiMax, lipofectamine 2000 or 3000, OPTI-MEM was purchased form Invitrogen. Bafilomycin A1, cycloheximide, doxycycline, imidazole, TPCK-Trypsin, 0.1% poly-L-lysine, fibronectin were purchased from Sigma Aldrich. Ni-NTA agarose resin was purchased from Qiagen. µCLEAR 96-well optical microplates plates (#655090) were purchased from Greiner Bio-one.

IAV reverse genetics

Reverse genetics using the 8 plasmid rescue system [29] (a kind of gift of Robert Webster) was performed as follows: per 60mm dish of HEK 293T cells, 1 µg each of purified plasmid DNA (i.e. pHW-2000-M, -NP, -HA, -NA, -PB1, -PB2, -PA,- NS1 (WSN)) were co-transfected using lipofectamine 2000. Eighteen h later the medium was exchanged to DMEM containing 0.2% BSA, 0.1% FCS, 2mM L-glutamine, 1µg/ml

TPCK-Trypsin. Virion-containing supernatants were harvested at 48 h post-transfection. The mutant virus and the corresponding WT virus was recovered in the medium of the transfected cells, and quantitated using an IIF-based cell binding assay.

siRNA transfections

siRNAs (AllStars Negative control, TNPO1#1 (Hs_TNPO1_7:CAGCATGTTAAGCCTTGTATA), TNPO1#2 (Hs_TNPO1_2:CAGAATTGGCCTGACCTCTTA), TNPO1#3 (Hs_TNPO1_6:CTGGAACAACTTAATCAGTAT), Hs_ATP6V1B2_3 (CACGGTTAATGAAGTCTGCTA), Hs_KPNB1_1 (TCGGTTATATTTGCCAAGATA) were purchased from Qiagen. Reverse transfection was done using Lipofectamine RNAiMax and OPTI-MEM at a final 10 nM siRNA concentration. The cells were maintained in a 5% CO_2 incubator at 37°C for 3 days before experiments were performed.

RNAi screening

Seventy host genes regulating nucleocytoplasmic transport (3 siRNAs per gene) were distributed across four plates in a 96-well plate format. siRNAs (10 µl of a 100 nM stock in OPTI-MEM; Invitrogen) were added to the transfection reagent (0.1 µl RNAiMax in 20 µl OPTI-MEM) in wells of 96-well plates and incubated at room temperature for 45 min. Then, 1,500 A549 cells were added to each well in 70 µl of growth medium. 62 h after transfection, cells were infected with MOI≈0.2-0.5 of IAV X31 in infection medium for 10 h. Cells were fixed with 4% formaldehyde in PBS, stained for NP, and DNA was stained with DAPI. Cells were automatically imaged using a 20× objective on a BD pathway 855 microscope. The percentage of infected cells was analysed by the Infection Counter, a MatLab-based program, as previously described [25]. The Allstars Negative Control was included three times on each plate. All siRNAs used for screening were designed by and purchased from Qiagen.

IAV entry, infection and replication assays

Virus assays were performed in infection medium (DMEM, 50 mM HEPES buffer, pH 6.8, 0.2% BSA). The virus entry assays were carried out as per the protocols previously described [1, 25]. The detection time-point for infection (NP expression) was 7 hpi. The assays were performed either in 24-well plates for confocal imaging (using 100× and 63× objectives) and FACS analysis, or 96-well optical bottom plates for automated imaging. For assays using MEFs the surface of plates/coverslips was coated with fibronectin (50 µg/ml in PBS) for 30 min prior to the experiment. Coverslips were mounted on slides with Immu-Mount (Thermo Fisher Scientific). For rescue experiments using A549 cells, siRNA TNPO1#2 was transfected using RNAiMax. Two days later an siRNA-resistant construct pEGFP-TNPO1 was transfected using lipofectamine 2000. Eighteen h later, the infection assay was performed and cells were fixed at 6.5 hpi, stained for NP and analysed by FACS. The proportion of NP-positive cells in the low to mid GFP-expressing population was analysed using the FlowJo software. High GFP-expressing cells were not analysed. For IAV replication assays, MDCK cells were induced of TNPO1 shRNA expression by the addition of 1 µg/ml doxycycline to the growth medium for 3 days. IAV X31 was then infected at MOI=0.01 for 1h after which the medium was replaced with MEM supplemented with 0.1% FCS, 0.2% BSA, 100 U/ml penicillin, 100 µg/ml streptomycin, 2 mM L-glutamine and 1 µg/ml TPCK-Trypsin. Supernatants were harvested at 24 hpi (and 48 hpi) and the infectious titer was analysed by $TCID_{50}$ on MDCK cells.

Synchronised penetration assay at LEs (NH_4Cl washout)

Cells grown on coverslips in 24-well or 4-well plates were bound with 1 µl of X31 (MOI≈100) per well in infection medium for 1 h on ice. The cells were washed and warmed to 37°C to allow endocytosis for 20 min in the presence of 1 mM cycloheximide, after which the medium was replaced with STOP medium (DMEM, 50 mM HEPES, pH adjusted to 7.4, supplemented with 20 mM NH_4Cl immediately before use)

and incubated further for 1 h to accumulate virus particles in the LEs. The medium was replaced with infection medium with cycloheximide to allow endosomal re-acidification and viral penetration and cells were fixed at indicated time points, and processed for IIF [1, 35].

Synchronised fusion assay at the plasma membrane (acid bypass)

Labeling of the virus with lipophilic fluorescent dyes (R18/SP-DiOC18(3)) was done as previously described [1, 25]. In brief, 50 µl of X31 stock was diluted in 750 µl PBS, to which a premixture of R18 and SP-DiOC18(3) was added with vigorous mixing, at a final concentration of 0.4 µM and 0.2 µM, respectively. The mixture was rocked for 1 h at room temperature in the dark, and filtered through a syringe filter with a 0.22 µm pore size (Millipore) to remove unbound dye and aggregates. Cells were trypsinised, counted and 50,000 cells were taken into each eppendorf tube in a volume of 50 µl. Fifty µl of R18/SP-DiOC18(3) labelled virus was added and the mixture was incubated on ice for 30 min with tapping every 10 min to allow for virus binding to cells. Cells were washed with cold infection medium by low speed centrifugation to remove unbound virus particles. After removal of the supernatant, 300 µl of pre-warmed pH 7.4 medium or medium buffered to pH 5.0 with 50 mM citrate buffer were added to the cells, mixed and incubated at 37°C in a water bath with circulation in a floating device. After 2 min, cells were fixed immediately by direct addition of 300 µl of 8% formaldehyde in PBS. After washing, the cells were resuspended in 250 µl of FACS buffer, and analysed by FACS.

Acid bypass M1-uncoating, vRNP nuclear import assays

To detect M1-uncoating and NP expression by inducing viral fusion at the plasma membrane, acid-bypass uncoating and infection assays were performed as previously described [1]. X31 stock (5 µl, MOI≈500 for uncoating assay and 2 µl, MOI≈200 for nuclear import assay/well of a 96-well optical plate) was pre-bound to cells on ice for 1 h. Cells were washed with cold infection medium to remove unbound virus. After removal of infection medium, 500 µl of pre-warmed pH 6.8 medium or medium buffered to pH 5.0 with

citrate buffer was added. The plates were incubated in a 37°C water bath on top of a metal block touching the plate bottom directly. After 2 min, the cells were washed 2 times with cold infection medium and incubated with STOP medium. Cells were further incubated at 37°C for 3 min for the M1-uncoating assay, or for 45 min for the nuclear import assay, on a prewarmed metal plate in 5% CO_2, 37°C, after which they were fixed and processed for confocal microscopy. M1-uncoating was detected by the characteristic increase in the immunostaining with anti-M1 monoclonal antibody (HB-64) after uncoating. For M1-uncoating rescue assays in TNPO1 shRNA-expressing MDCK cells, pEGFP-TNPO1 or pEGFP-C3 (control) constructs was transfected 2 days after shRNA induction by doxycycline. Twenty h after transfection, cells were trypsinised, counted and 30,000 cells were taken in each eppendorf tube in a volume of 50 µl. Three µl (MOI≈100) of X31 in 50 µl infection medium was added to the cells, mixed and incubated on ice for 30 min with occasional tapping. Cells were washed with cold infection medium by low speed centrifugation to remove unbound virus particles. After removal of the supernatant, 300 µl of pre-warmed pH 6.8 medium or medium buffered to pH 5.0 with 50 mM citrate buffer were added to the cells and incubated at 37°C for 2 min in a water bath with circulation on a floating device. Further, 300 µl of pre-warmed pH 6.8 medium or pH 8 medium (to re-neutralise the pH 5.0 medium) was added, and incubated for 3 min at 37°C. Cells were fixed by directly adding 600 µl of 8% formaldehyde in PBS. After washing, the cells were resuspended in 250 µl of FACS buffer, stained with HB-64 (1:3000) and analysed by FACS.

Recombinant protein purification

His-tagged human TNPO1 was expressed at 21°C in SG13 bacterial cells. The cell pellet was lysed by French Press twice and incubated with Ni-NTA agarose for 2 h at 4°C [36]. The purified protein was eluted with imidazole-containing buffer (50 mM Na_2HPO_4, 250 mM NaCl, 400 mM imidazole, 5 mM β-EtSH) followed by gel filtration in gel filtration buffer (10 mM HEPES pH 7.5, 150 mM NaCl, 1 mM DTT) with a Superdex 200 10/300 GL column (GE Healthcare). His-tagged MBP proteins were purified from pOPINM-HisMBP-mouse HDAC6 constructs. Mouse HDAC6 proteins were expressed in Sf9 insect cells

and purified with Ni-NTA agarose (Qiagen) and gel filtration with a Superdex 200 16/60 column. Purified protein was digested with 3C protease (Sigma Aldrich) overnight on ice, then purified with Amylose resin (NEB). After the 3C cleavage step, His-tagged MBP was eluted from the resin with 10 mM maltose-containing buffer (20 mM Tris-HCl, pH 7.5, 200 mM NaCl, 10 mM maltose, 2 mM TCEP) and gel filtrated in gel filtration buffer (20 mM Tris, pH 7.5, 200 mM NaCl, 2 mM TCEP).

Pull-down assay from purified IAV extracts

Purified IAV X31 was treated with/without priming for 30 min at 37°C using either neutral buffer (30 mM HEPES, 30 mM MES, pH 7) or priming buffer (30 mM MES pH 5.6, 120 mM KCl) [6]. After priming, IAV were lysed with Cytoskeleton (CSK) buffer (10 mM PIPES pH 6.8, 100 mM NaCl, 300 mM Sucrose, 3 mM $MgCl_2$, 1 mM EGTA, 0.1% Triton X-100) supplemented with a protease inhibitor cocktail (Roche). Lysis was performed by incubating for 30 min on ice with occasional pipetting. The lysed virus was used for Ni-NTA agarose pull-down analysis. Four µg of purified His-tagged human TNPO1 protein was mixed with the virus lysate. Purified His-tagged maltose binding protein (MBP) was used as negative control. The mixture was incubated for 3 h at 4°C on a rotary shaker after which 20 µl of a 50% slurry of Ni-NTA agarose beads (equilibrated with CSK buffer containing 20 mM imidazole and 1% BSA) was added and rotated for 30 min at 4°C. The samples were spun down at 3,000 rpm for 1 min at 4°C, beads were washed once with CSK buffer containing 20 mM imidazole, 1% BSA, followed by two washes in CSK buffer containing 20 mM imidazole. Finally, the precipitate was eluted with 15 µL of CSK buffer containing 200 mM imidazole. The samples were lysed in Laemmli buffer and boiled for 5 min at 95°C, and loaded onto a Bolt™ 4-12% Bis-Tris Plus Gel (Thermo Fisher Scientific), and run in MES running buffer for 35 min at 200 V. The protein samples were transferred onto immobilon-P PVDF membranes (Merck) using a Trans-Blot SD Semi-Dry Electrophoretic Transfer Cell (Bio-rad) according to instructions by the manufacturer. After transfer, the PVDF membrane was washed for 5 min in 1x TBST buffer, then blocked with 5% skim milk (Sigma) in 1xTBS buffer for 1 h at room temperature. Primary antibodies against M1 (HB-64) and/or

His-tag were used at 1:3000 and 1:1000 dilution, respectively. The primary antibody reaction was carried out at 4°C overnight, then the membrane was washed three times with 1x TBST buffer for 5 min each. Secondary antibodies (anti-mouse IgG-HRP conjugated or anti-goat IgG-HRP conjugated) were used at 1:3000 dilution in 5% skim milk in 1x TBS buffer and incubated for 1 h at room temperature and washed with 1x TBST buffer three times for 15 min each. The signal was detected using SuperSignal™ West Pico PLUS Chemiluminescent Substrate (Thermo Fisher Scientific), exposed on an X-ray film (Fuji Film) and developed with a developer machine.

Immunoprecipitation assay

A549 cells growing in 60 mm dishes were washed with infection medium and bound with 10µl (MOI≈50) of X31 for 45 min on ice. The cells were washed and incubated in warm infection medium or STOP medium at 37°C for 2.5 h, after which the cells were washed in PBS, harvested with a cell scraper and centrifuged at 3,000 rpm for 5 min using a benchtop microcentrifuge. The supernatant was removed and the cell pellet was lysed in 100µl of CSK buffer, sonicated and incubated for 60 min on ice with occasional vortexing. The lysate was centrifuged at 3,000 rpm for 5 min after which the supernatant was reacted with anti-TNPO1 antibody (mouse, 1 µg) or mouse IgG (1 µg) and rotated for 2 h at 4°C. Then, 20 µl of a 1:1 slurry of Protein A/G Agarose (Pierce) in CSK buffer was added and rotated for 1 h at 4°C. The beads were washed three times in CSK buffer by pelleting at 3,000 rpm for 5 min at 4°C, and processed for SDS-PAGE and Western blotting as described for the pull-down assay.

Molecular cloning

Plasmid constructs used were pEGFP-M9NLS, -M9NLS mutant and pQE-Trn1[36]. pEGFP-TNPO1 was a kind gift of Woan-Yuh Tarn. To generate the TNPO1#2-resistant construct pEGFP-TNPO1-Res1, a primer (GCAACAAAAACTGGAACAACTGAATCAGTATCCAGAC) was used to introduce a silent point

mutation into the pEGFP-TNPO1 sequence by mutagenesis PCR. GFP-M1 was constructed by inserting IAV (A/WSN/1933(H1N1) M1 WT sequence amplified by PCR using the primer pair (fwd: CGCCTCGAGATGAGTCTTCTAACCGAGGTCGAA, rev: GGAATTCTCACTTGAATCGTTGCATCTGC), into the pEGFP-C3 vector via XhoI/EcoRI restriction sites. The point mutations G18A, P19A, L20A, K21A were further introduced using the GFP-M1 as template: The primers used for each point mutant were G18A (fwd: GTCCCGTCAGcCCCCCT, rev:GATAGAGAGAACGTACGTTTCGACCTC), P19A (fwd: CCCGTCAGGCgCCCTCAAAGC, rev: ACGATAGAGAGAACGTACGTTTCGACCTC), L20A (fwd: GTCAGGCCCCgcCAAAGCCGAG, rev: GGGACGATAGAGAGAACGTACGTTTCGACC), K21A (fwd: GGCCCCCTCgcAGCCGAGATCG, rev: TGACGGGACGATAGAGAGAACGTACGTTTC). All constructs were verified by sequencing.

Cloning, expression and purification of G18A M1-N

A DNA template encoding matrix protein M1 from IAV A/WSN/1933(H1N1) (GenBank accession number CY034133.1) was gene synthesised by GeneArt. The G18A M1 1-158 (G18A M1-N) sequence was generated by PCR and cloned into pOPINF using In-Fusion cloning [37]. This construct, pOPINF G18A M1-N, yields an N-terminal His x6 tag with a 3C protease site followed by the M1-N sequence that corresponds to Uniprot P05777 except for the single point mutation G18A. Protein expression was performed in *E.coli* BL21 DE3 cells via auto-induction at 20°C. Cell extracts were obtained using an EmulsiFlex-C3 (Avestin) cell disruptor and clarified via centrifugation and filtration. The target protein was first purified over nickel Superflow (Qiagen) resin followed by gel filtration on a S75 HiLoad 16/60 column (GE Healthcare). His-tagged G18A M1-N protein was concentrated to 9.1 mg/ml in 20 mM Tris, pH 7.5, 200 mM NaCl, 2 mM TCEP and 0.02% NaN_3.

Crystallisation, data collection and structure determination

N-terminally His-tagged IAV M1 protein consisting of residues 1-158 (M1-N) was crystallised using the sitting-drop vapor diffusion method at 20°C with a Phoenix nano-liter dispensing robot (Art Robbins). One hundred nl of M1-N protein at 9.1 mg/ml in protein buffer (0.02 M Tris, pH 7.5, 0.2 M NaCl, 2 mM TCEP, 0.02% NaN_3) was mixed with 100 nl of crystallisation buffer (30 % (w/v) EDO_P8K, 0.1 M MB2 pH 7.5, 10% NPS; Molecular Dimensions Morpheus HT-96 C6). Long rod-like crystals were obtained after 5-10 days, which were harvested and cryo-cooled in liquid nitrogen. X-ray data collection was carried out at the SLS PX-II beamline in Villigen, Switzerland, at 100 K. IAV M1-N protein crystals diffracted to 1.9 Å and belonged to space group P1 at pH 7.5 with two molecules per unit cell. Diffraction data was integrated and scaled using the XDS program package [38] and the M1-N structure was solved by the molecular replacement method with PHASER [39] using available wild-type M1 structures as search models. The structure was then manually completed and further improved by the crystallographic simulated annealing routine followed by individual B-factor refinement in PHENIX [40]. The structure was finalized by several rounds of manual rebuilding in COOT and refinement in BUSTER [41]. Structure validation was carried out using tools implemented in COOT. Structural images for figures were prepared with PyMOL (https://pymol.org). Atomic coordinates and structure factors have been deposited in the Protein Data Bank under accession code 6I3H.

Image acquisition

For the initial RNAi screening, automated image acquisition was performed using 96-well optical bottom plates with a BD Pathway microscope using a 10x objective. Subsequent automated image acquisition was performed with a 10x objective using Molecular Devices ImageXpress Micro imaging system or Yokogawa CV7000. Four (2x2) to 9 (3x3) images were acquired from each well for each fluorescence channel depending on the instrument, typically resulting in the counting of more than 3,000 cells in the control sample. High-resolution images were acquired on inverted microscopes Zeiss LSM 510 Meta, LSM 780,

Leica SP8 for confocal imaging, or Deltavision OMX for structured illumination super-resolution microscopy (SIM).

Image analysis

Images were processed in Cell Profiler 3.0.0 to identify areas of M1, NP and LAMP1 signal and to measure the intensity and shape parameters of these objects for colocalisation analysis. Briefly, images were median filtered to remove noise and objects were identified in the M1, NP and LAMP1 channels using an adaptive Otsu thresholding method. The M1 and NP objects were masked by the identified LAMP1 objects to create images showing M1 or NP signals from within or outside of LAMP1-positive regions. The intensity, shape and location of these objects were then measured. To identify individual cells, the signals from the M1, NP and LAMP1 channels were added together and smoothed with a Gaussian filter creating a smoothed integrated intensity image of all the three signals. The Hoechst stained cell nuclei were then identified as objects and used as the seed points to distinguish cell boundaries using the previously created smoothed integrated intensity image. Measurement of M1 and NP object intensities were then made inside and outside of the nuclei area. The individual identified M1 and NP objects were then combined for each image to create a mask of all M1 and/or NP signal areas inside or outside of LAMP1 signal areas, and then these were dilated by 2 pixels. Colocalisation analysis (rank-weighted) was then performed using the raw M1 and NP images masked by either of these masks.

Phenotypic analysis of the M1 uncoating dataset was performed by supervised machine learning software, the Advanced Cell Classifier [25]. Confocal images for analysis were acquired using a 63× oil (NA 1.40) objective at 1024×1024 pixels per image with a Leica SP8 microscope.

Statistical analysis

Data are represented as mean ± SD. For all analyses, multiple independent experiments (N≥3) were carried out. Statistical analysis was performed using Prism 7 (GraphPAD Software Inc.) software.

Data availability

The data that support the findings of this study are available from the corresponding author upon request. Atomic coordinates and structure factors of G18A M1-N have been deposited in the Protein Data Bank under accession code 6I3H.

References

1. Banerjee, I. *et al.* Influenza A virus uses the aggresome processing machinery for host cell entry. *Science* **346**, 473-477 (2014).
2. Lee, B.J. *et al.* Rules for nuclear localization sequence recognition by karyopherin beta 2. *Cell* **126**, 543-558 (2006).
3. Noda, T. & Kawaoka, Y. Packaging of influenza virus genome: robustness of selection. *Proceedings of the National Academy of Sciences of the United States of America* **109**, 8797-8798 (2012).
4. Yamauchi, Y. & Greber, U.F. Principles of Virus Uncoating: Cues and the Snooker Ball. *Traffic* **17**, 569-592 (2016).
5. Helenius, A. Virus Entry: Looking Back and Moving Forward. *Journal of molecular biology* **430**, 1853-1862 (2018).
6. Stauffer, S. *et al.* Stepwise priming by acidic pH and a high K+ concentration is required for efficient uncoating of influenza A virus cores after penetration. *J Virol* **88**, 13029-13046 (2014).
7. Matlin, K.S., Reggio, H., Helenius, A. & Simons, K. Infectious entry pathway of influenza virus in a canine kidney cell line. *J Cell Biol* **91**, 601-613 (1981).
8. White, J., Kartenbeck, J. & Helenius, A. Membrane fusion activity of influenza virus. *EMBO J* **1**, 217-222 (1982).
9. Maeda, T., Kawasaki, K. & Ohnishi, S. Interaction of influenza virus hemagglutinin with target membrane lipids is a key step in virus-induced hemolysis and fusion at pH 5.2. *Proceedings of the National Academy of Sciences of the United States of America* **78**, 4133-4137 (1981).
10. Eisfeld, A.J., Neumann, G. & Kawaoka, Y. At the centre: influenza A virus ribonucleoproteins. *Nature reviews. Microbiology* **13**, 28-41 (2015).
11. Whittaker, G., Bui, M. & Helenius, A. Nuclear trafficking of influenza virus ribonuleoproteins in heterokaryons. *J Virol* **70**, 2743-2756 (1996).
12. Martin, K. & Helenius, A. Transport of incoming influenza virus nucleocapsids into the nucleus. *J Virol* **65**, 232-244 (1991).
13. Martin, K. & Helenius, A. Nuclear transport of influenza virus ribonucleoproteins: the viral matrix protein (M1) promotes export and inhibits import. *Cell* **67**, 117-130 (1991).
14. O'Neill, R.E., Jaskunas, R., Blobel, G., Palese, P. & Moroianu, J. Nuclear import of influenza virus RNA can be mediated by viral nucleoprotein and transport factors required for protein import. *The Journal of biological chemistry* **270**, 22701-22704 (1995).
15. Kemler, I., Whittaker, G. & Helenius, A. Nuclear import of microinjected influenza virus ribonucleoproteins. *Virology* **202**, 1028-1033 (1994).
16. Chou, Y.Y. *et al.* Colocalization of different influenza viral RNA segments in the cytoplasm before viral budding as shown by single-molecule sensitivity FISH analysis. *PLoS Pathog* **9**, e1003358 (2013).

17. Hao, R. *et al.* Proteasomes activate aggresome disassembly and clearance by producing unanchored ubiquitin chains. *Molecular cell* **51**, 819-828 (2013).
18. Wild, T. *et al.* A protein inventory of human ribosome biogenesis reveals an essential function of exportin 5 in 60S subunit export. *PLoS biology* **8**, e1000522 (2010).
19. Badertscher, L. *et al.* Genome-wide RNAi Screening Identifies Protein Modules Required for 40S Subunit Synthesis in Human Cells. *Cell reports* **13**, 2879-2891 (2015).
20. Fried, H. & Kutay, U. Nucleocytoplasmic transport: taking an inventory. *Cellular and molecular life sciences : CMLS* **60**, 1659-1688 (2003).
21. Konig, R. *et al.* Human host factors required for influenza virus replication. *Nature* **463**, 813-817 (2010).
22. Pollard, V.W. *et al.* A novel receptor-mediated nuclear protein import pathway. *Cell* **86**, 985-994 (1996).
23. Siomi, H. & Dreyfuss, G. A nuclear localization domain in the hnRNP A1 protein. *J Cell Biol* **129**, 551-560 (1995).
24. Bogerd, H.P. *et al.* Definition of a consensus transportin-specific nucleocytoplasmic transport signal. *The Journal of biological chemistry* **274**, 9771-9777 (1999).
25. Banerjee, I., Yamauchi, Y., Helenius, A. & Horvath, P. High-content analysis of sequential events during the early phase of influenza A virus infection. *PloS one* **8**, e68450 (2013).
26. White, J., Kartenbeck, J. & Helenius, A. Fusion of Semliki forest virus with the plasma membrane can be induced by low pH. *J Cell Biol* **87**, 264-272 (1980).
27. Soniat, M. & Chook, Y.M. Karyopherin-beta2 Recognition of a PY-NLS Variant that Lacks the Proline-Tyrosine Motif. *Structure* **24**, 1802-1809 (2016).
28. Harris, A., Forouhar, F., Qiu, S., Sha, B. & Luo, M. The crystal structure of the influenza matrix protein M1 at neutral pH: M1-M1 protein interfaces can rotate in the oligomeric structures of M1. *Virology* **289**, 34-44 (2001).
29. Hoffmann, E., Neumann, G., Kawaoka, Y., Hobom, G. & Webster, R.G. A DNA transfection system for generation of influenza A virus from eight plasmids. *Proceedings of the National Academy of Sciences of the United States of America* **97**, 6108-6113 (2000).
30. Arzt, S. *et al.* Combined results from solution studies on intact influenza virus M1 protein and from a new crystal form of its N-terminal domain show that M1 is an elongated monomer. *Virology* **279**, 439-446 (2001).
31. Chiang, M.J. *et al.* Maintaining pH-dependent conformational flexibility of M1 is critical for efficient influenza A virus replication. *Emerg Microbes Infect* **6**, e108 (2017).
32. Zhang, Y. *et al.* Mice lacking histone deacetylase 6 have hyperacetylated tubulin but are viable and develop normally. *Molecular and cellular biology* **28**, 1688-1701 (2008).
33. Hurd, T.W., Fan, S. & Margolis, B.L. Localization of retinitis pigmentosa 2 to cilia is regulated by Importin beta2. *J Cell Sci* **124**, 718-726 (2011).
34. Nohinek, B., Gerhard, W. & Schulze, I.T. Characterization of host cell binding variants of influenza virus by monoclonal antibodies. *Virology* **143**, 651-656 (1985).
35. Singh, I.R., Suomalainen, M., Varadarajan, S., Garoff, H. & Helenius, A. Multiple mechanisms for the inhibition of entry and uncoating of superinfecting Semliki Forest virus. *Virology* **231**, 59-71 (1997).
36. Guttinger, S., Muhlhausser, P., Koller-Eichhorn, R., Brennecke, J. & Kutay, U. Transportin2 functions as importin and mediates nuclear import of HuR. *Proceedings of the National Academy of Sciences of the United States of America* **101**, 2918-2923 (2004).
37. Berrow, N.S., Alderton, D. & Owens, R.J. The precise engineering of expression vectors using high-throughput In-Fusion PCR cloning. *Methods in molecular biology* **498**, 75-90 (2009).
38. Kabsch, W. Integration, scaling, space-group assignment and post-refinement. *Acta Crystallogr D Biol Crystallogr* **66**, 133-144 (2010).
39. McCoy, A.J. *et al.* Phaser crystallographic software. *J Appl Crystallogr* **40**, 658-674 (2007).
40. Afonine, P.V. *et al.* phenix.model_vs_data: a high-level tool for the calculation of crystallographic model and data statistics. *J Appl Crystallogr* **43**, 669-676 (2010).
41. Bricogne G., B.E., Brandl M., Flensburg C., Keller P., Paciorek W., & Roversi P, S.A., Smart O.S., Vonrhein C., Womack T.O. BUSTER version X.Y.Z.
. (2017).

Figure Legends

Fig.1 TNPO1 is required for IAV infection.

(a) Heatmap showing the top 19 hit genes (out of 70) from the nucleocytoplasmic transport factor siRNA screen. The screen was repeated independently three times using IAV X31 strain in A549 cells. The read-out for infection was done by IIF against NP (HB-65). The average infection inhibition of individual siRNAs, and that of the three independent siRNAs are shown.

(b) IAV infection is reduced in TNPO1-depleted cells. A549 cells treated with AllStars Neg control siRNA or with siTNPO1 or siATP6V1B2 (a vacuolar-ATPase subunit, used as a positive control) were infected with IAV and stained for NP (HB-65) at 10 h.p.i. Scale bars; 200 µm. Nuclei were stained with DAPI. The experiments were repeated independently multiple times (n>3) with similar results.

(c) Reduced IAV infection in A549 cells transfected with siTNPO1#2 or siATP6V1B2. TNPO1-depletion was confirmed by Western blotting. n=3 biologically independent experiments. P value was determined using two-sided, unpaired t-test.

(d) Reduced IAV infection in MDCK cells expressing TNPO1 shRNA. TNPO1-depletion was confirmed by Western blotting. n=4 biologically independent experiments. P value was determined using two-sided, unpaired t-test.

(e) Reduced IAV replication in TNPO1-depleted MDCK cells. Three days after TNPO1 shRNA induction by doxycycline, the cells were infected with X31 (MOI=0.01) after which the supernatant was harvested at 24 hpi and the IAV titre was determined by $TCID_{50}$ assay. n=3 biologically independent experiments.

(f) IAV infection is rescued in TNPO1-depleted A549 cells by an siTNPO1-insensitive construct expressing GFP-TNPO1. n=3 biologically independent experiments.

(g) TNPO1 is required for infection of multiple IAV strains. siRNA-treated cells were infected with X31 (H3N2), WSN (H1N1), and Udorn (H3N2) strains. siATP6V1B2 was used as a positive control. n=3 biologically independent experiments. All bar graphs show the mean and SD.

Fig.2 TNPO1 promotes M1-uncoating from incoming cytoplasmic vRNPs.

(a) TNPO1-depletion inhibits M1-uncoating. M1 (HB-64) staining of IAV-infected A549 cells at 3 hpi. Scale bars; 10 µm. n=3 independent experiments gave similar results.

(b) IAV vRNP debundling can occur in the cytoplasm prior to vRNPs reaching the nuclear pore. NP (HB-65) staining of MEFs 1 h after synchronous penetration from LEs were imaged by SIM. Blow-up of the nucleus and of two areas (i, ii) are shown. Scale bars; 10 µm. n=3 independent experiments gave similar results.

(c) TNPO1-depletion inhibits vRNP nuclear import. NP (HB-65) staining of IAV-infected A549 cells at 4 hpi. Scale bars; 10 µm. n=3 independent experiments gave similar results.

(d) TNPO1 promotes M1-removal from cytoplasmic NP. Confocal images of IAV-infected A549 cells at 3 hpi. stained with Hoechst (grey), NP (HB-65, green), M1 (polyclonal, red) and LAMP1 (blue). The insets (i, ii) show blow-ups of areas selected by broken-line square(s). Scale bars; 10 µm. n=3 independent experiments gave similar results.

(e) Incoming M1 and NP colocalise in the cytoplasm of TNPO1-depleted cells. IAV-infected A549 cells (n=15) at 2.5 hpi were stained as in (d), imaged, and analysed automatically. The rank-weighted colocalisation index of M1 and NP spots excluding LAMP1 and nucleus is shown. n=2 independent experiments.

(f) Cytoplasmic NP area is increased in TNPO1-depleted cells. IAV-infected A549 cells (n=15) at 2 and 2.5 hpi were processed as in (e). n=2 independent experiments gave similar results. The mean and SD are shown.

(g) Cytoplasmic M1 intensity is increased in TNPO1-depleted cells. IAV-infected A549 cells (n=15) at 2 and 2.5 hpi were processed as in (e). The experiments were repeated independently twice with similar results. The mean with 95% CI is shown. P value was determined using two-sided, unpaired t-test.

(h) TNPO1 promotes M1-bypass uncoating. A549 cells were subjected to acid bypass fusion/hemifusion, M1-uncoating and vRNP import assays. The percentage of cells positive for DiOC18(3), dispersed M1 (HB-64) staining, and nuclear NP was quantified for the fusion assay, M1 uncoating assay, and vRNP import assay, respectively. The mean and SD are shown (n=3).

(i) Acid bypass IAV fusion/hemifusion is unaffected in TNPO1-depleted MDCK cells. Bypass (-)/(+) indicates pH 6.8- or pH 5.0-treated samples, respectively. Performed 3 days after shRNA induction. The mean is shown (n=2).

(j) Acid bypass M1-uncoating is blocked in TNPO1-depleted MDCK cells. The mean and SD are shown (n=5).

(k) Ectopic expression of GFP-human TNPO1 rescues acid bypass M1-uncoating in TNPO1-depleted MDCK cells. After 2 days of shRNA-induction cells were transfected with GFP or GFP-TNPO1, and subjected to acid bypass M1-uncoating assay 20 h later. The mean and SD are shown (n=3). P value was determined using two-sided, unpaired t-test.

Fig. 3 TNPO1 binds to incoming IAV cores via a M1 N-terminal PY-NLS.

(a) TNPO1 colocalises with incoming M1 and NP. Fifteen min after synchronous LE penetration in MEFs or HDAC6 -/- MEFs, cells were stained for TNPO1 (magenta), NP (HB-65, green), and M1 (polyclonal, cyan). Locations indicated by arrowheads are blown-up in the inset. Scale bars; 10 µm. n=3 independent experiments gave similar results.

(b) TNPO1 co-precipitates with M1 from primed IAV. Purified X31 virions were non-primed (pH 7.0) or primed (pH 5.6, 120 mM[K^+]) and subjected to a His-TNPO1 pull-down assay, analysed by SDS-PAGE and Western blotting. His-MBP was used as a negative control. n=3 independent experiments gave similar results.

(c) Sequence alignment of known PY-NLSs with the conserved IAV M1 N-terminal sequence. Epitope 1 (a hydrophobic patch, containing the glycine), 2 (a basic patch) and 3 (PY) was adapted from [2, 27].

(d) Glycine 18 is critical for IAV infection. IAV WSN strains (WT or G18A) were reverse genetically produced to infect A549 cells. Their infectivity was analysed by IIF against NP (HB-65). The mean and SD are shown (n=3). P value was determined using two-sided, unpaired t-test.

(e) TNPO1 co-precipitates less efficiently with M1 from G18A virus compared to WT virus. Viruses were primed and precipitated with His-TNPO1 as in (b), and detected by SDS-PAGE and Western blotting. n=2 independent experiments gave similar results.

(f) Structure of G18A compared to WT M1-N (L1/L3 loops). Superposition of M1-N structures present in the Protein Data Bank that crystallised in the neutral pH face-to-back arrangement. G18A M1-N is shown as grey cartoon with selected residues as sticks in atom colours. PDB entries 1EA3 [30] and 5V8A [31] are shown as cartoon models in blue and gold, respectively, with selected residues displayed as lines.

(g) Detailed view of the G18A mutation with its electron density. L1/L3 loops of G18A M1-N are shown as sticks in grey and atom colours. A $2mF_o$-DF_c simulated annealing omit electron density map is displayed in blue (1σ).

(h) Surface representation of the L1-L3 region of M1-N highlighting the closing of a surface cavity in M1-N G18A (grey, left) if compared with 1EA3 (blue, right).

Fig. 4

Model of step-wise IAV uncoating by HDAC6 and TNPO1 during cell entry. After viral uptake into endosomes, the M2 cation channels open resulting in influx of protons and K^+ ions that loosens interactions stabilising the core. This triggers a conformational change in M1 that exposes the PY-NLS close to the N-terminus. Following viral fusion in LEs, the core is exposed to cytosolic factors and HDAC6 binds to shell-associated, unanchored ubiquitin chains via its zinc finger ubiquitin-binding domain (ZnF-UBP). HDAC6 N-terminus binds to M1. Together with other components of the aggresome processing machinery such as motors dynein, myosin II, microtubules and actin filaments, HDAC6 releases the M1 shell from the

endosome surface and ruptures it. The eight bundled vRNPs are released into the cytosol. At the same time, TNPO1 associates with the PY-NLS exposed in the primed M1. TNPO1 removes residual M1 from the vRNP surface, which allows the dissociation of vRNPs from each other. KPNA and KPNB1 bind to the classical NLS in NP resulting in nuclear import of fully or partially debundled vRNPs. MTOC; microtubule organising centre. The figure was adapted from[1].

Figure 1

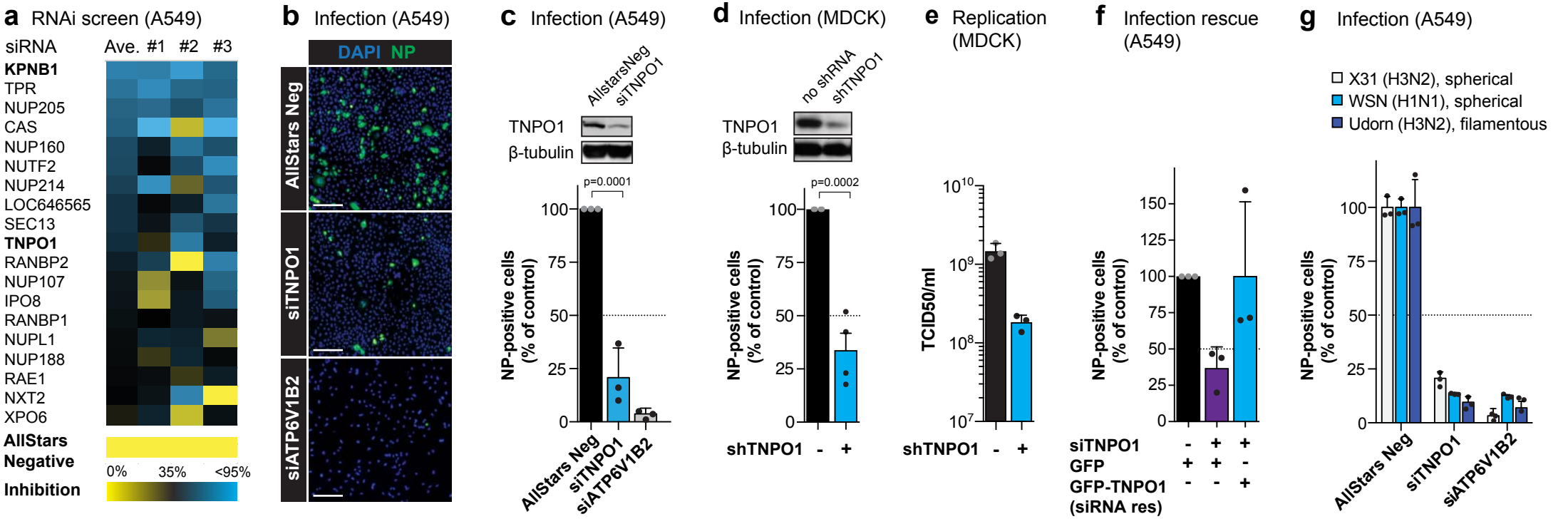
a RNAi screen (A549)
siRNA
Ave. #1 #2 #3
KPNB1
TPR
NUP205
CAS
NUP160
NUTF2
NUP214
LOC646565
SEC13
TNPO1
RANBP2
NUP107
IPO8
RANBP1
NUPL1
NUP188
RAE1
NXT2
XPO6
AllStars Negative
0% 35% <95%
Inhibition
b Infection (A549)
DAPI NP
AllStars Neg
siTNPO1
siATP6V1B2
c Infection (A549)
AllStarsNeg
siTNPO1
TNPO1
β-tubulin
p=0.0001
NP-positive cells (% of control)
AllStars Neg
siTNPO1
siATP6V1B2
d Infection (MDCK)
no shRNA
shTNPO1
TNPO1
β-tubulin
p=0.0002
NP-positive cells (% of control)
shTNPO1 - +
e Replication (MDCK)
TCID50/ml
shTNPO1 - +
f Infection rescue (A549)
NP-positive cells (% of control)
siTNPO1 - + +
GFP + + -
GFP-TNPO1 (siRNA res) - - +
g Infection (A549)
X31 (H3N2), spherical
WSN (H1N1), spherical
Udorn (H3N2), filamentous
NP-positive cells (% of control)
AllStars Neg
siTNPO1
siATP6V1B2

Figure 2

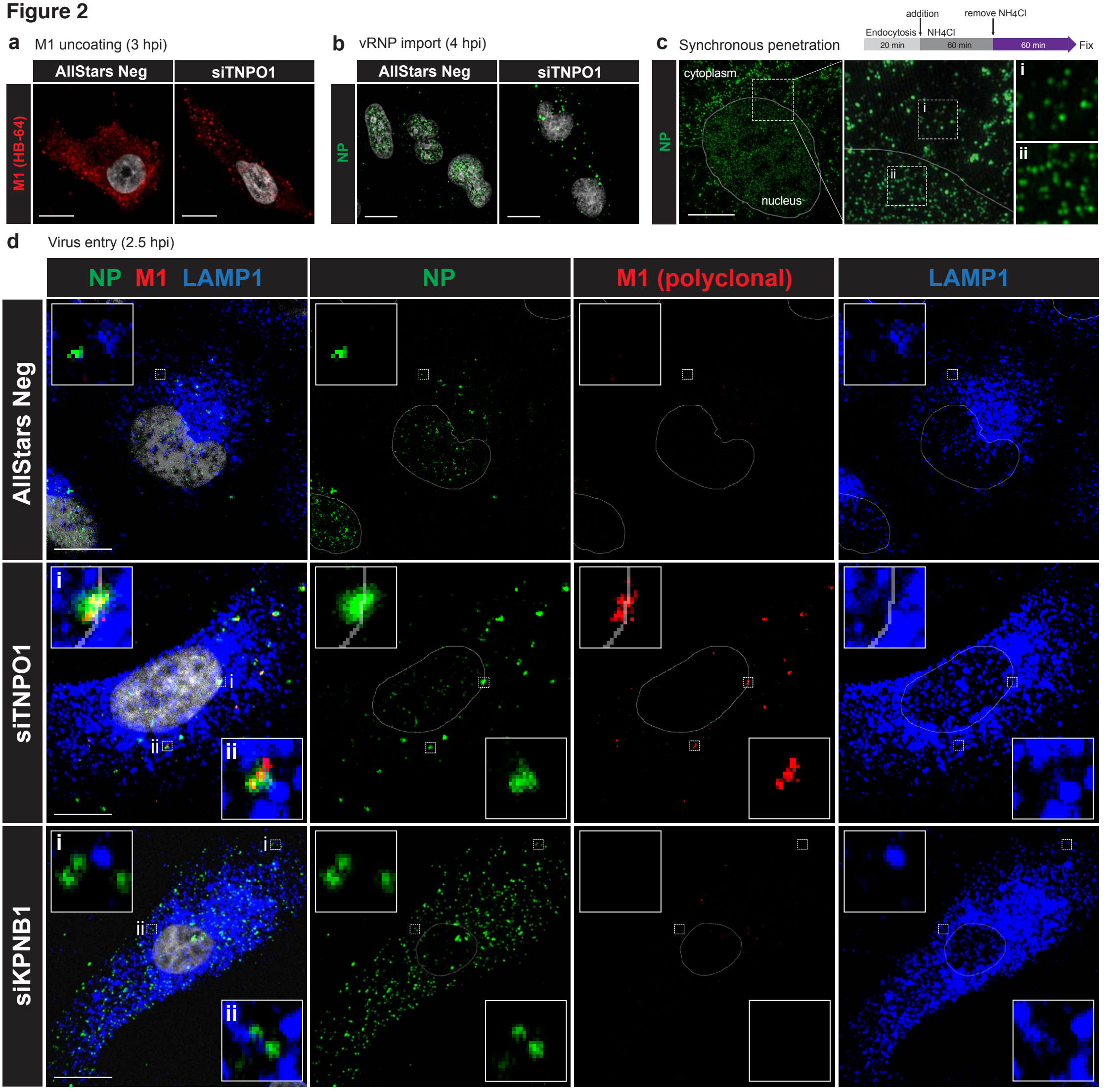
a
M1 uncoating (3 hpi)
AllStars Neg
siTNPO1
M1 (HB-64)
b
vRNP import (4 hpi)
AllStars Neg
siTNPO1
NP
c
Synchronous penetration
addition
remove NH4Cl
Endocytosis
NH4Cl
20 min
60 min
60 min
Fix
NP
cytoplasm
nucleus
i
ii
d
Virus entry (2.5 hpi)
NP M1 LAMP1
NP
M1 (polyclonal)
LAMP1
AllStars Neg
siTNPO1
siKPNB1

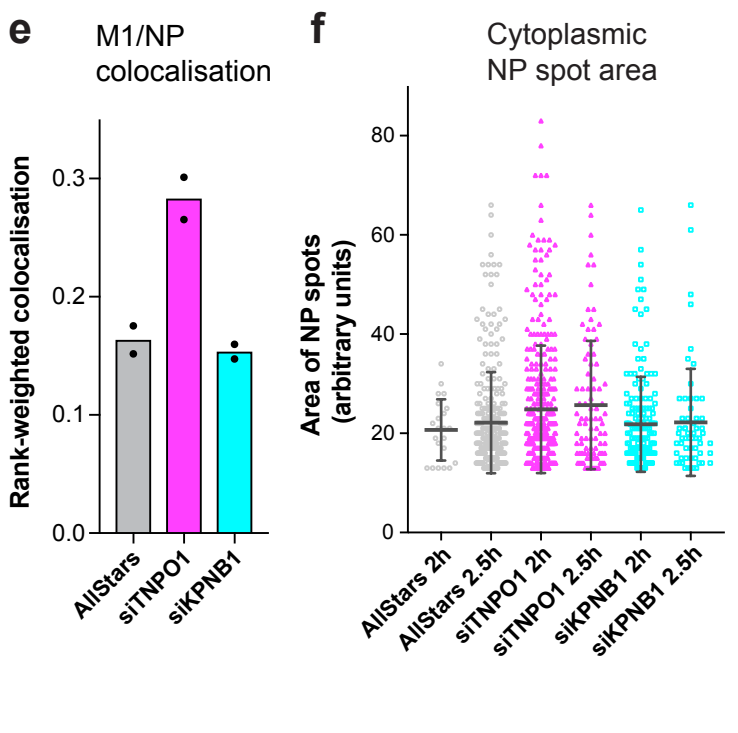
e
M1/NP colocalisation
Rank-weighted colocalisation
0.0
0.1
0.2
0.3
AllStars
siTNPO1
siKPNB1

f
Cytoplasmic NP spot area
Area of NP spots (arbitrary units)
0
20
40
60
80
AllStars 2h
AllStars 2.5h
siTNPO1 2h
siTNPO1 2.5h
siKPNB1 2h
siKPNB1 2.5h

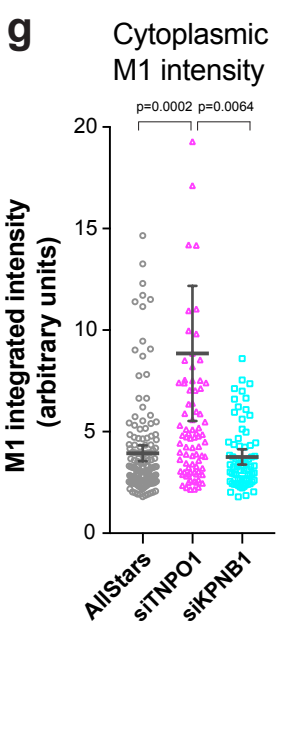
g
Cytoplasmic M1 intensity
M1 integrated intensity (arbitrary units)
p=0.0002
p=0.0064
0
5
10
15
20
AllStars
siTNPO1
siKPNB1

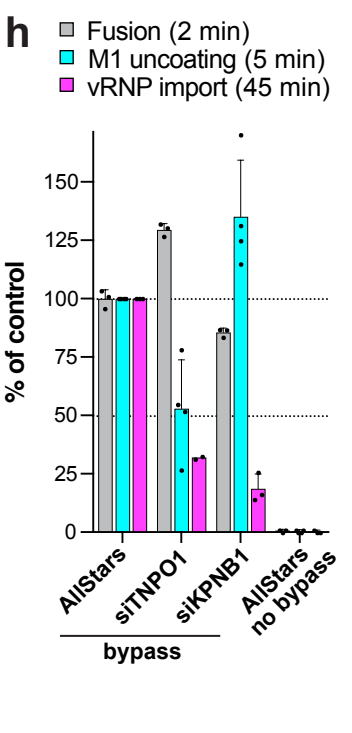
h
Fusion (2 min)
M1 uncoating (5 min)
vRNP import (45 min)
% of control
0
25
50
75
100
125
150
AllStars
siTNPO1
siKPNB1
AllStars no bypass
bypass

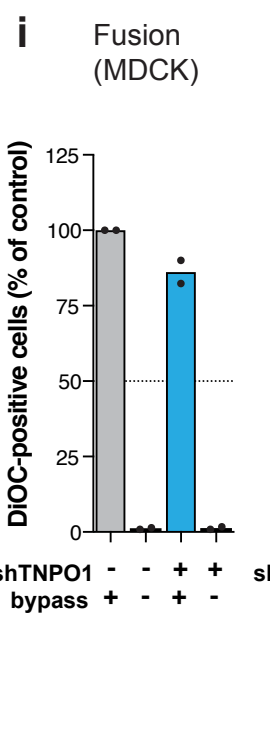
i
Fusion (MDCK)
DiOC-positive cells (% of control)
0
25
50
75
100
125
shTNPO1 - - + +
bypass + - + -

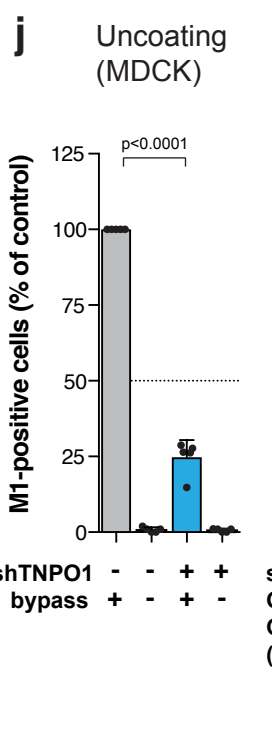
j
Uncoating (MDCK)
p<0.0001
M1-positive cells (% of control)
0
25
50
75
100
125
shTNPO1 - - + +
bypass + - + -

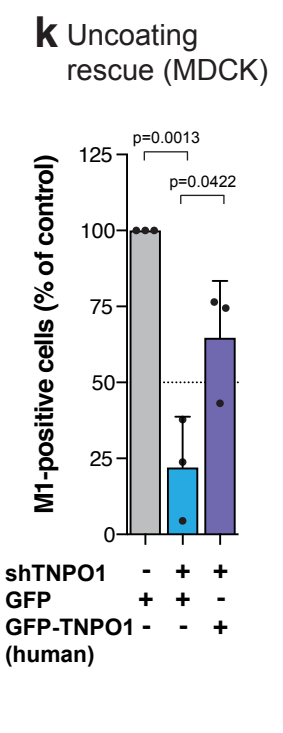
k
Uncoating rescue (MDCK)
p=0.0013
p=0.0422
M1-positive cells (% of control)
0
25
50
75
100
125
shTNPO1 - + +
GFP + + -
GFP-TNPO1 (human) - - +

Figure 3

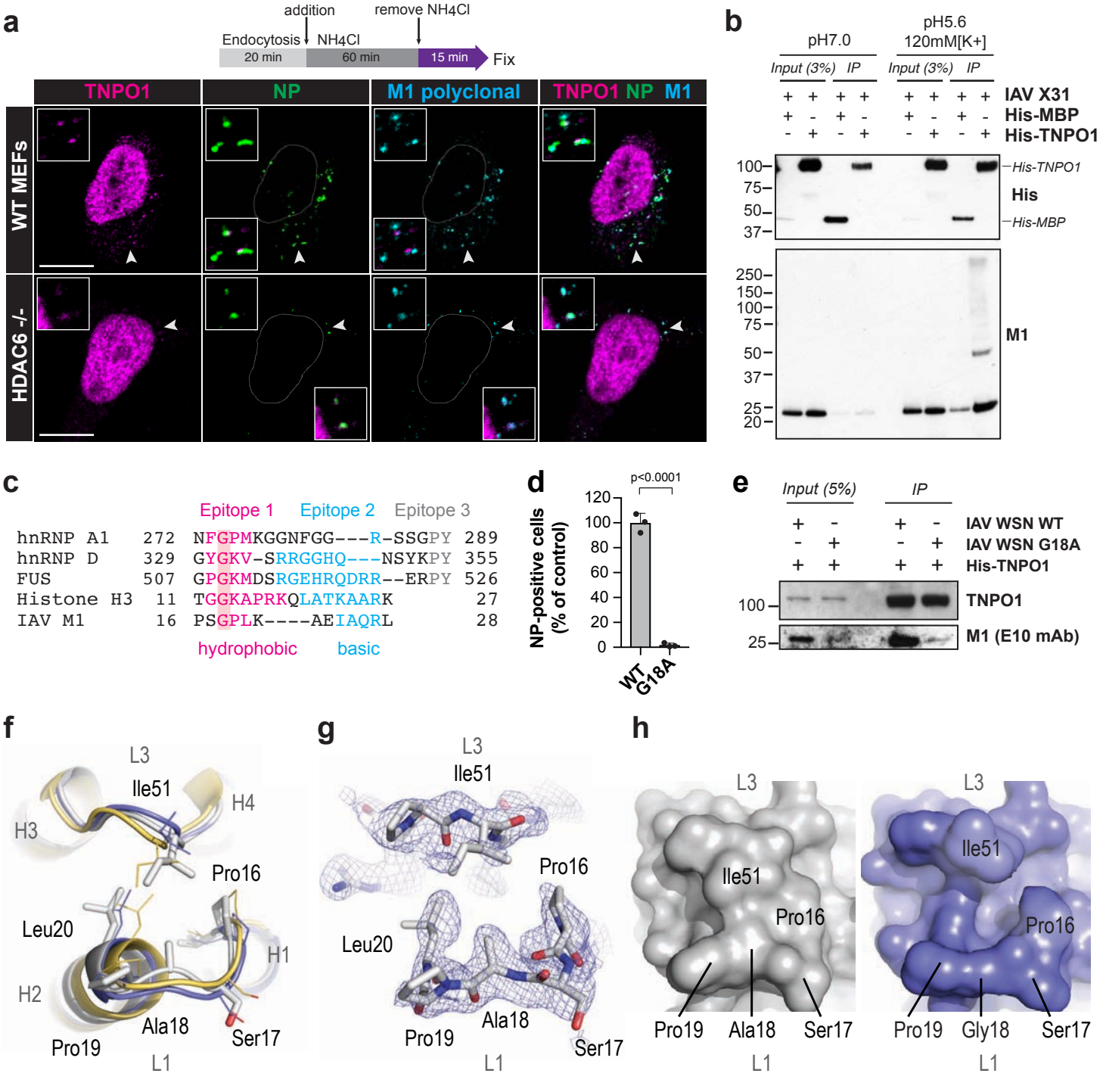
a
addition
remove NH4Cl
Endocytosis
NH4Cl
20 min
60 min
15 min
Fix
TNPO1
NP
M1 polyclonal
TNPO1 NP M1
WT MEFs
HDAC6 -/-
b
pH7.0
pH5.6
120mM[K+]
Input (3%)
IP
IAV X31
His-MBP
His-TNPO1
His-TNPO1
His
His-MBP
M1
c
Epitope 1
Epitope 2
Epitope 3
hnRNP A1 272 NFGPMKGGNFGG---R-SSGPY 289
hnRNP D 329 GYGKV-SRRGGHQ---NSYKPY 355
FUS 507 GPGKMDSRGEHRQDRR--ERPY 526
Histone H3 11 TGGKAPRKQLATKAARK 27
IAV M1 16 PSGPLK----AEIAQRL 28
hydrophobic
basic
d
p<0.0001
NP-positive cells (% of control)
WT
G18A
e
Input (5%)
IP
IAV WSN WT
IAV WSN G18A
His-TNPO1
TNPO1
M1 (E10 mAb)
f
L3
Ile51
H4
H3
Pro16
Leu20
H1
H2
Ala18
Pro19
Ser17
L1
g
L3
Ile51
Pro16
Leu20
Ala18
Pro19
Ser17
L1
h
L3
Ile51
Pro16
Pro19
Ala18
Ser17
L1
L3
Ile51
Pro16
Pro19
Gly18
Ser17
L1

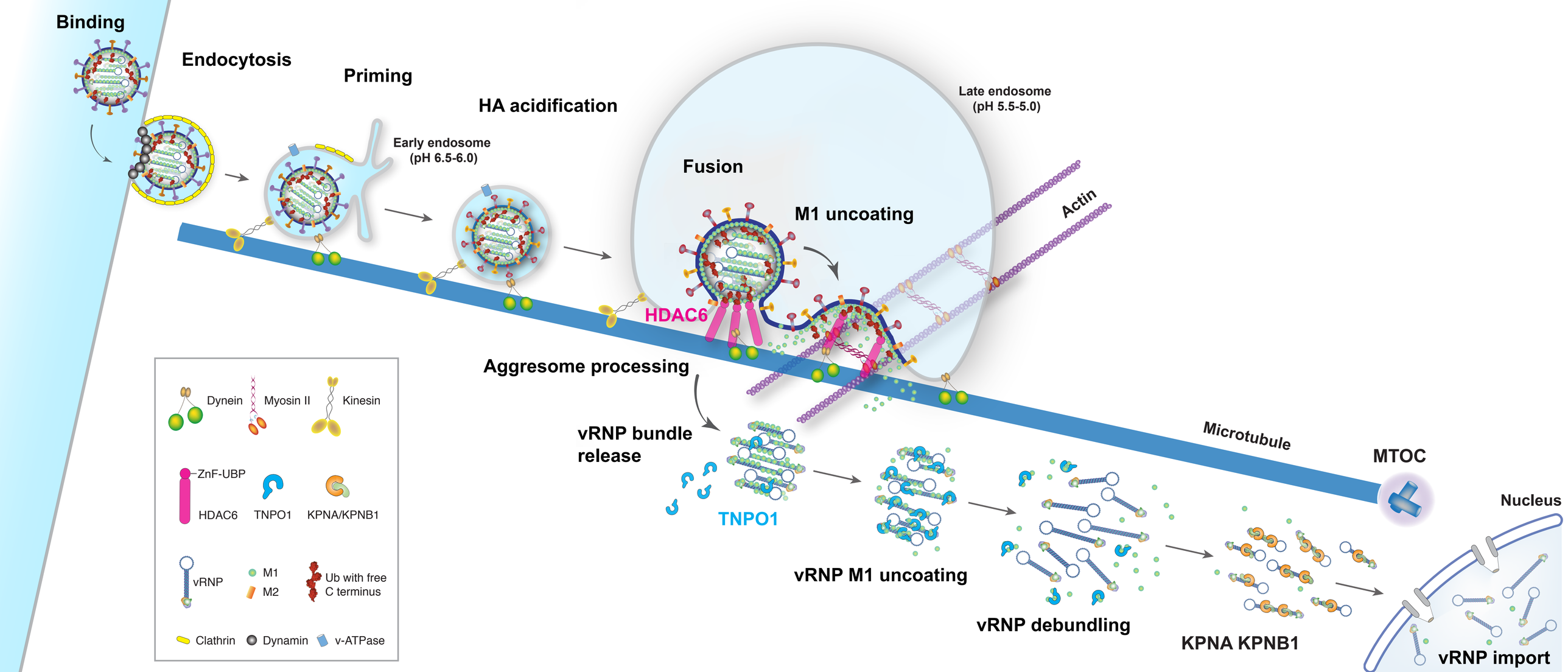
Binding
Endocytosis
Priming
HA acidification
Early endosome
(pH 6.5-6.0)
Late endosome
(pH 5.5-5.0)
Fusion
M1 uncoating
Actin
HDAC6
Aggresome processing
vRNP bundle
release
TNPO1
vRNP M1 uncoating
vRNP debundling
KPNA KPNB1
Microtubule
MTOC
Nucleus
vRNP import
Dynein
Myosin II
Kinesin
ZnF-UBP
HDAC6
TNPO1
KPNA/KPNB1
vRNP
M1
M2
Ub with free
C terminus
Clathrin
Dynamin
v-ATPase

Supplementary Information

Influenza Virus Uses Transportin 1 for vRNP Debundling During Cell Entry

Yasuyuki Miyake[1,4], Jeremy Keusch[3], Laure Decamps[2†], Hung Ho-Xuan[2†], Sho Iketani[1], Heinz Gut[3], Ulrike Kutay[2], Ari Helenius[2], Yohei Yamauchi[1*]

Affiliations:

[1]School of Cellular and Molecular Medicine, Faculty of Life Sciences, University of Bristol, University Walk, Bristol, BS8 1TD, UK.

[2]Institute of Biochemistry, ETH Zurich, Otto-Stern-Weg 3, CH-8093, Zurich Switzerland.

[3]Friedrich Miescher Institute for Biomedical Research, Maulbeerstrasse 66, 4058 Basel, Switzerland

[4]Department of Virology, Nagoya University Graduate School of Medicine, 65 Tsurumai-cho, Showa-ku, Nagoya 466-8550, Aichi, Japan.

*email: yohei.yamauchi@bristol.ac.uk

†These authors contributed equally to this work.

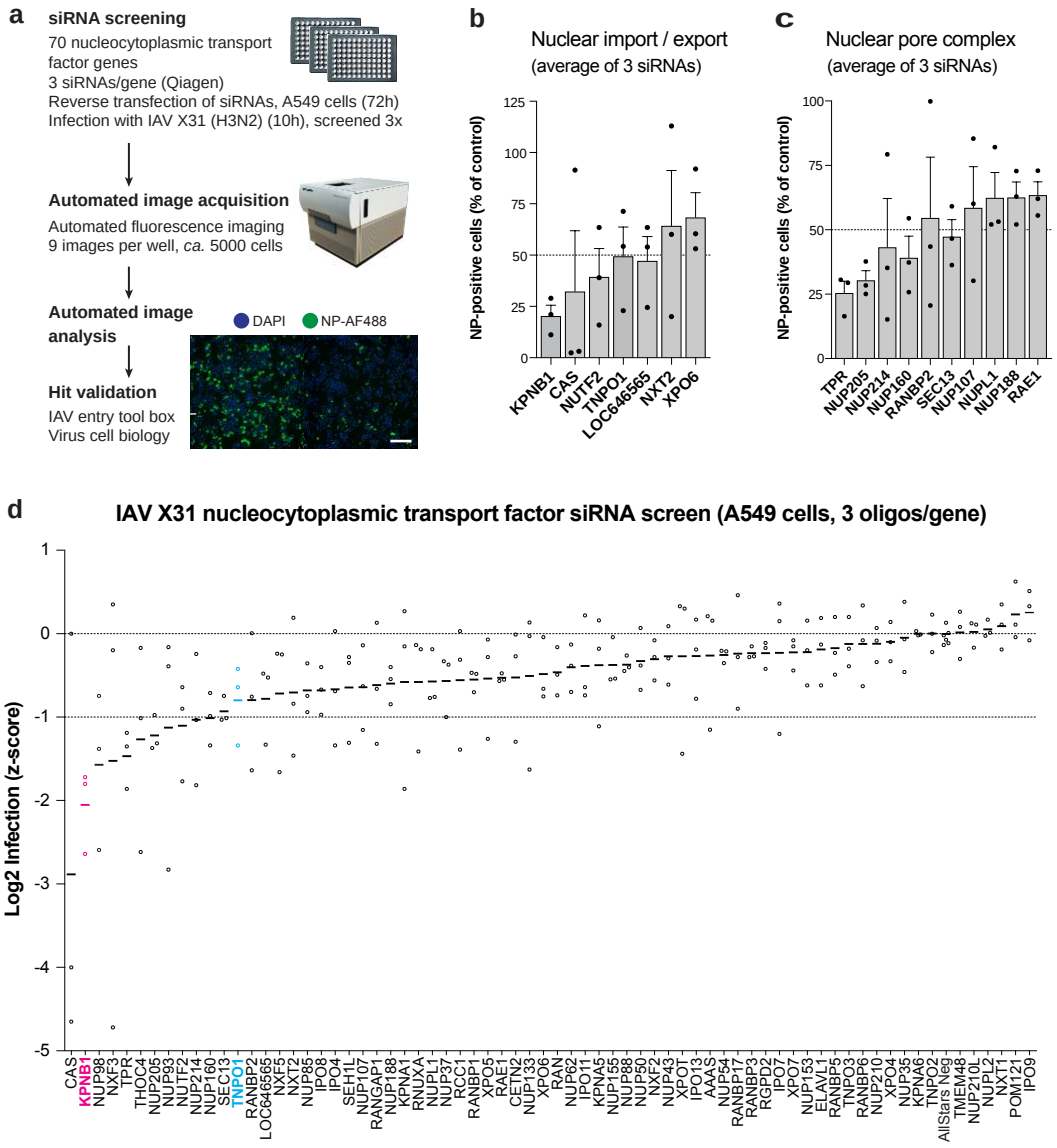

Supplementary Figure 1

Nucleocytoplasmic transport factor siRNA screen against IAV X31 in A549 cells. (a) The workflow of the nucleocytoplasmic transport factor siRNA screen performed in A549 cells using IAV X31 (an H3N2 reassorted strain derived from PR8 and A/Hong Kong/1/68 strains). Scale bar; 200 μm. (b) The import/export factor genes and (c) nuclear pore component genes that decreased IAV infection. Genes that were toxic upon depletion were removed. The mean and SD of the results of infection compared to control cells after depletion with three different siRNA oligos are shown. n=3 independent experiments. (d) The full list of genes targeted in the siRNA screen and the results of IAV infection upon their depletion. The average z-score value (log2 infection compared to the control) of the three different siRNA oligos are shown per gene.

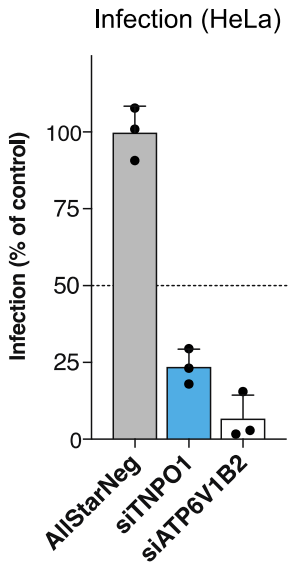

Supplementary Figure 2

TNPO1 is required for IAV X31 infection in HeLa cells. Cells were treated with AllStars Negative control, TNPO1, ATP6V1B2 siRNAs and infected with X31, fixed at 10 hpi. IAV infection was analysed by IIF against NP (HB-65). n=3 independent experiments. The mean and SD are shown.

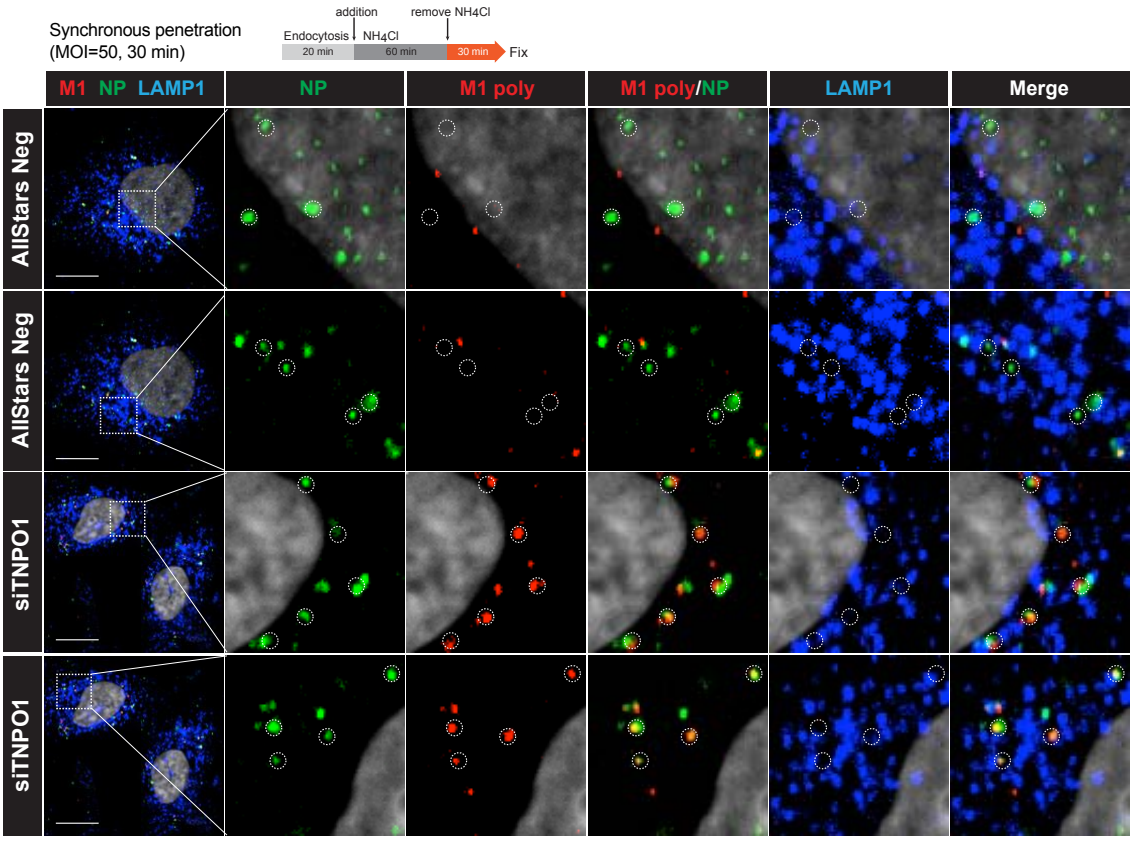

Supplementary Figure 3

TNPO1 promotes removal of residual M1 from penetrated cytoplasmic vRNPs. IAV (MOI=50) was allowed to enter A549 cells transfected with AllStars Negative control or TNPO1#3 siRNAs, subjected to synchronous LE penetration and fixed after 30 min. The cells were processed for IIF and stained for NP (HB-65, green), M1 (polyclonal, red) and LAMP1 (blue). The open-lined circles indicate cytoplasmic NP spots devoid of significant LAMP1 staining, and their respective locations in the other two (red, blue) channels. The nuclei were stained with Hoechst (grey). Scale bars; 10 µm. The experiments were repeated independently three times with similar results.

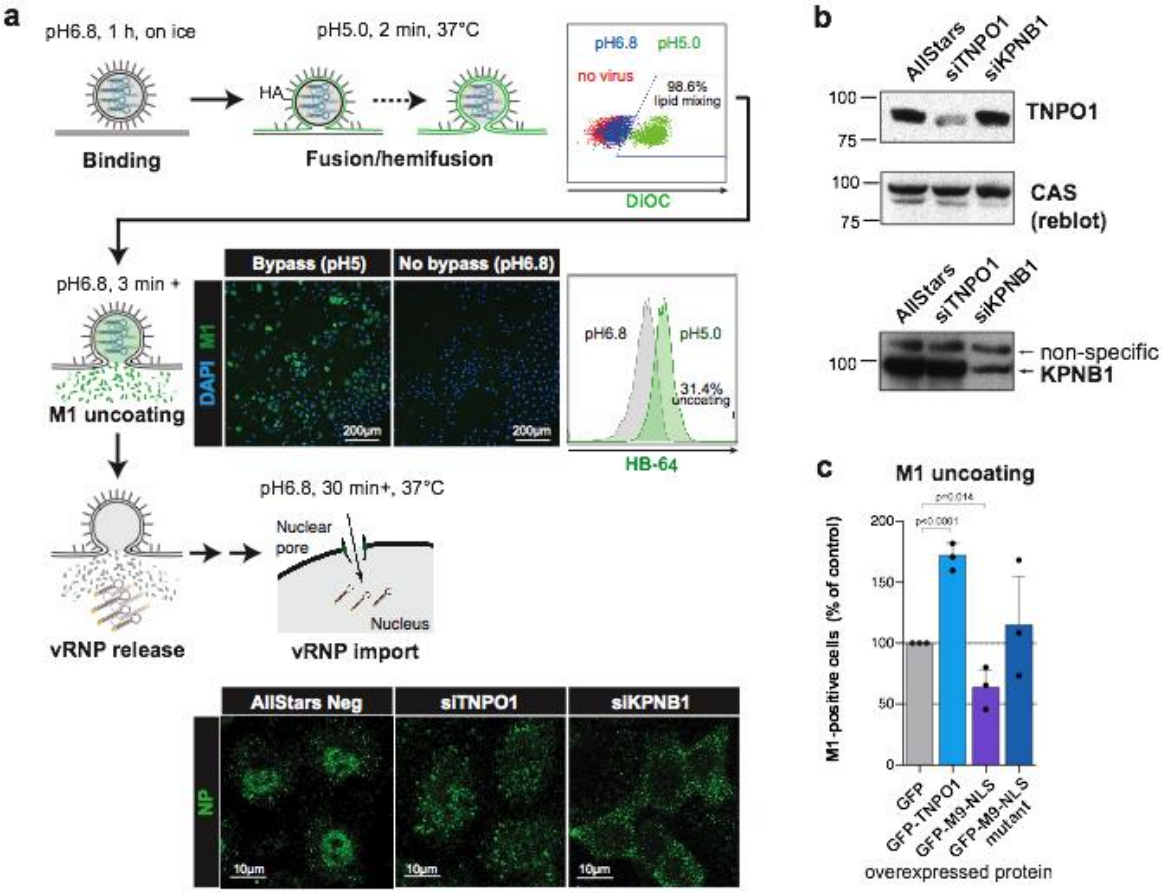

Supplementary Figure 4

M9-NLS competes with TNPO1 for M1-uncoating. (a) Schematic showing the steps of acid bypass IAV entry assays i.e. fusion/hemifusion, M1-uncoating, vRNP import, and the representative data derived. (b) Depletion of TNPO1 and KPNB1 in A549 cells transfected with siRNAs. A549 cells were transfected with siRNAs for 3 days after which they were harvested and analysed by SDS-PAGE and Western blotting. The membrane used for TNPO1 detection was reblotted to detect CAS (which served as a loading control). For the KPNB1 blot, a non-specific band served as a loading control. The experiments were repeated three times with similar results. (c) TNPO1 overexpression increases M1-uncoating, whereas hnRNP A1 M9-NLS overexpression reduces M1-uncoating. The acid bypass M1-uncoating assay was performed in A549 cells transiently expressing GFP, GFP-TNPO1, GFP-M9-NLS, or GFP-M9-NLS mutant. The cells were fixed 3 min after the pH 5.0 acid pulse, processed for IIF against M1 (HB-64) and the percentage of M1-positive cells were analysed by FACS. The P values were determined by two-sided, unpaired t-test. The mean and SD are shown.

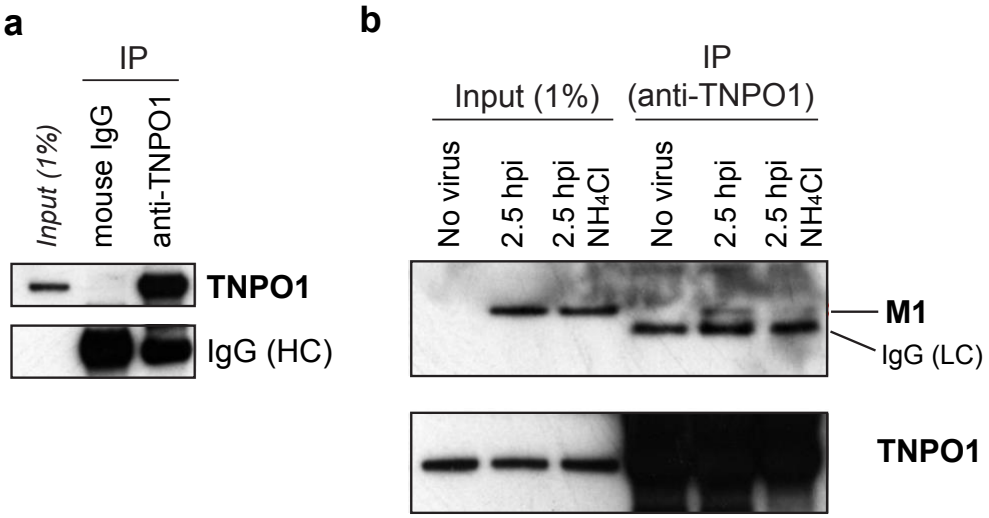

Supplementary Figure 5

TNPO1 co-precipitates with incoming IAV M1. (a) A549 cells were lysed and immunoprecipitated with anti-TNPO1 monoclonal antibody or mouse IgG as a negative control, subjected to SDS-PAGE, Western blotting and detected with anti-TNPO1. The IgG heavy chain (HC) is shown as a loading control. (b) IAV X31 was bound to A549 cells for 45 min on ice, washed, and incubated at 37°C in the absence or presence of 20mM NH_4Cl for 2.5 h and lysed in CSK buffer. The lysates were immunoprecipitated with anti-TNPO1 monoclonal antibody, subjected to SDS-PAGE, Western blotting, and detected with M1 (HB-64) and anti-TNPO1 antibodies. The experiments were repeated independently twice with similar results.

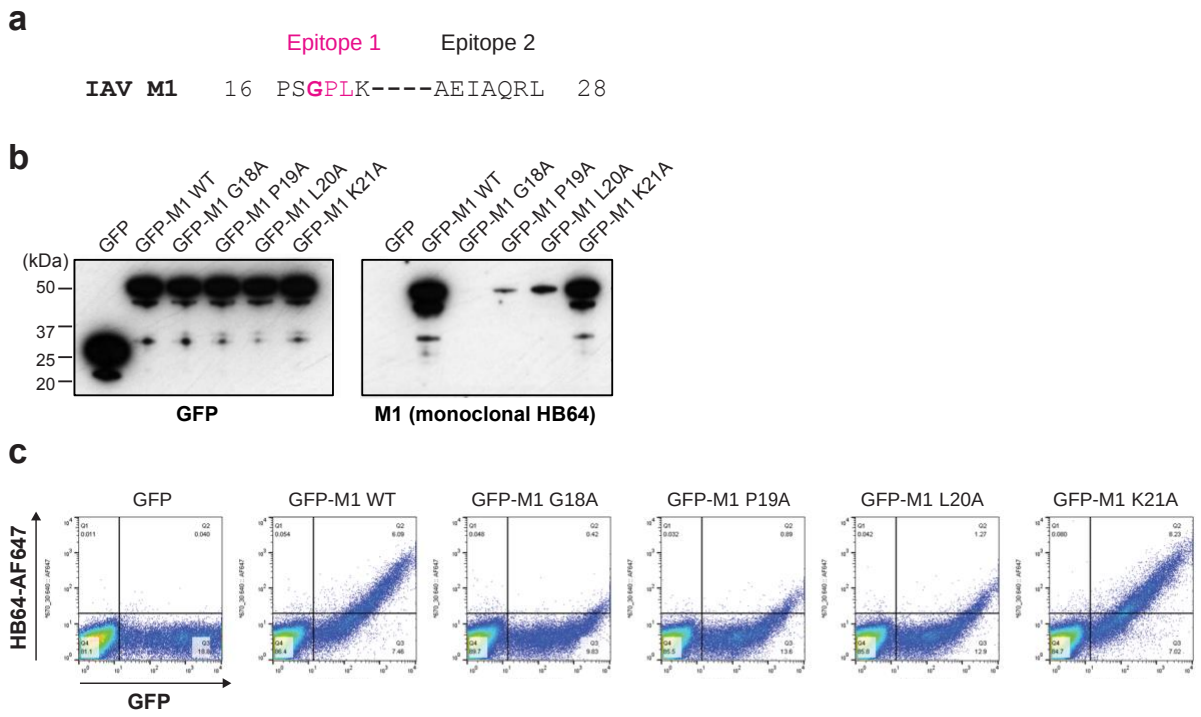

Supplementary Figure 6

IAV M1 N-terminus PY-NLS is the epitope of M1 monoclonal antibody HB-64 used for the M1-uncoating assay. (a) The IAV M1 N-terminal sequence showing epitope 1 and 2 of the PY-NLS. (b) Gly18 (and Pro19, Leu20 to a lesser degree) is the critical residue for M1 recognition by HB-64. Plasmids with single amino acid mutations in the hydrophobic patch (18-GPL-20) of epitope 1 were generated. HEK293T cells were transfected with plasmids expressing GFP-M1 WT, GFP-M1 G18A, GFP-M1 P19A, GFP-M1 L20A or GFP-M1 K21A and harvested 24 h later. The cell lysates were subjected to SDS-PAGE and Western blotting, and detected with anti-GFP and anti-M1 (HB-64) antibodies. (c) HEK293T cells were transfected with the same plasmids as in (b) for 24 h, after which they were trypsinised, fixed, processed for FACS after staining with HB-64 and anti-mouse Alexa Fluor 647 secondary antibody. The scatter plots depict GFP (x-axis) and HB-64 (y-axis) signal intensity. The experiments were repeated independently three times with similar results.

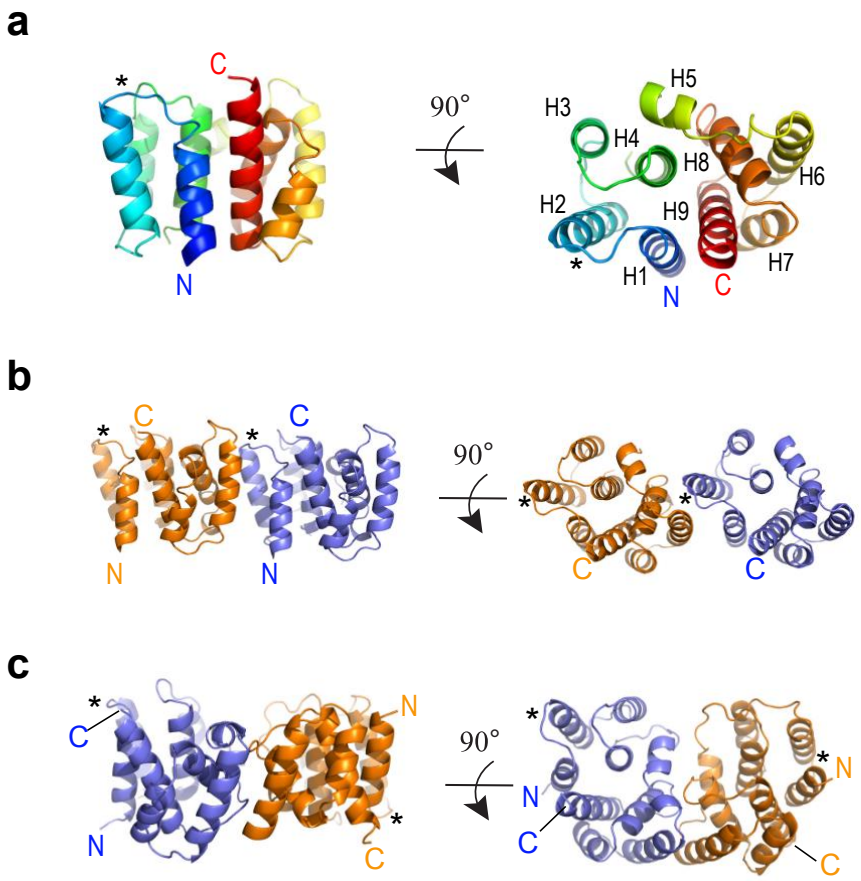

Supplementary Figure 7

Structure of G18A M1-N. (a) Overall structure of the G18A M1 N-terminal domain. The structure is displayed in cartoon mode in two orientations rotated by 90° around the indicated axis and colored in rainbow colors from blue (N-terminus) to red (C-terminus) to highlight the topology. N-, C-termini, and helices are labeled. The position of the G18A mutation is labeled with an asterisk. (b) Neutral pH, crystallographic face-to-back dimer of the G18A M1 N-terminal domain. The homodimer is presented as cartoon in two orientations rotated by 90° around the indicated axis. Monomers are colored in orange and blue. N-, C-termini, and the position of the G18A mutation are labeled. Parts of the structured N-terminal affinity tag are omitted for clarity reasons. (c) Acidic pH, face-to-face dimer of the M1 N-terminal domain as present in PDB entry 1AA7[1]. The homodimer is presented as cartoon in two orientations rotated by 90° around the indicated axis. Monomers are colored in orange and blue. N-, C-termini, and the position of the G18A mutation are labeled.

Table 1

Crystallographic Data Collection and Refinement Statistics

	M1-N G18A
Data collection	
Space group	P1
Unit cell dimensions	
a, *b*, *c* (Å)	35.56, 35.58, 69.29
α, β, γ (°)	89.71, 84.40, 69.02
Resolution range (Å)[a]	50.00-1.90 (1.95-1.90)
Wavelength (Å)	1.000
Completeness (%)[a]	94.6 (93.6)
Redundancy[a]	1.96 (1.95)
R_{sym}[a]	0.048 (0.371)
$I/\sigma(I)$[a]	9.69 (2.15)
CC (1/2) (%)[a]	99.7(80.4)
Unique reflections	23546
Refinement	
R_{work}	0.206
R_{free}	0.233
Resolution range (Å)	21.37 – 1.90
Reflections (all)	23530
Reflections (test set)	1177 (5%)
Number of atoms	
Overall	2675
Protein	2512
Solvent	163
***B*-Factors** (Å^2)	
Overall	44.4
Protein	44.1
Solvent	50.2
RMS Deviations	
Bond lengths (Å)	0.01
Bond angles (°)	1.03
Ramachandran plot	
Allowed (%)	99.3
Outliers (%)	0.7

[a]Values in parentheses refer to the highest resolution shell

Supplementary Figure 8

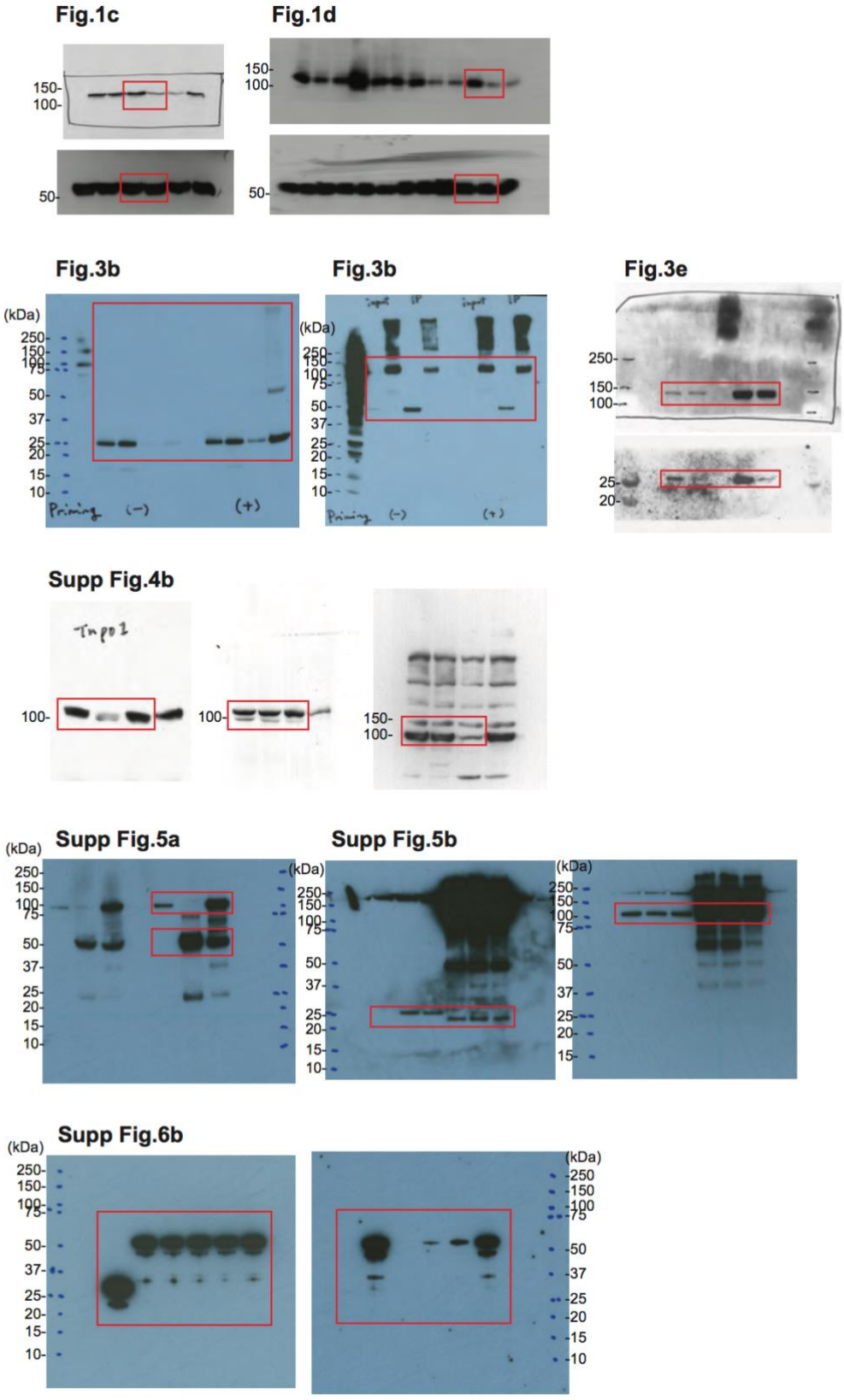

Supplementary References:

1. Sha, B. & Luo, M. Structure of a bifunctional membrane-RNA binding protein, influenza virus matrix protein M1. *Nature structural biology* **4**, 239-244 (1997).